Chapter 3

Zero-Dimensional Nanostructures: Nanoparticles

3.1. Introduction

Many techniques, including both top-down and bottom-up approaches, have been developed and applied for the synthesis of nanoparticles. Top-down approaches include milling or attrition, repeated quenching, and lithography. Attrition can produce nanoparticles ranging from a couple of tens to several hundreds nanometer in diameter. However, nanoparticles produced by attrition have a relatively broad size distribution and varied particle shape or geometry. In addition, they may contain a significant amount of impurities from the milling medium and defects resulted from milling. Such prepared nanoparticles are commonly used in the fabrication of nanocomposites and nanograined bulk materials, which requires much lower sintering temperatures. In nanocomposites and nanograined bulk materials, defects may be annealed during sintering, size distribution, particle shape, and a small amount of impurities are relatively insensitive for their applications. Repeated thermal cycling may also break a bulk material into small pieces, if the material has a very small thermal conductivity but a large volume change as a function of temperature. A big volume change associated with phase transition can be effectively utilized in this approach. Although very fine particles can be produced, this process is difficult to design and control so as to produce the desired particle size and shape. It is also limited to materials with very poor thermal conductivity but a large volume change. Lithography is another method to make small particles.[1,2]

Bottom-up approaches are far more popular in the synthesis of nanoparticles and many methods have been developed. For example,

nanoparticles are synthesized by homogeneous nucleation from liquid or vapor, or by heterogeneous nucleation on substrates. Nanoparticles or quantum dots can also be prepared by phase segregation through annealing appropriately designed solid materials at elevated temperatures. Nanoparticles can be synthesized by confining chemical reactions, nucleation and growth processes in a small space such as micelles. Various synthesis methods or techniques can be grouped into two categories: thermodynamic equilibrium approach and kinetic approach. In the thermodynamic approach, synthesis process consists of (1) generation of supersaturation, (2) nucleation, and (3) subsequent growth. In the kinetic approach, formation of nanoparticles is achieved by either limiting the amount of precursors available for the growth such as used in molecular beam epitaxy, or confining the process in a limited space such as aerosol synthesis or micelle synthesis. In this chapter, the attention will be focused mainly on the synthesis of nanoparticles through thermodynamically equilibrium approach. However, some typical kinetic approaches such as microemulsion, aerosol pyrolysis, and template-based deposition, will be highlighted as well. For the thermodynamic equilibrium approach, this chapter will take the solution synthesis of nanoparticles as an example to illustrate the fundamental requirements and consideration, however the fundamentals and principles are applicable to other systems without or with minimal modification.

For the fabrication of nanoparticles, small size is not the only requirement. For any practical application, the processing conditions need to be controlled in such a way that resulting nanoparticles have the following characteristics: (1) identical size of all particles (also called monosized or with uniform size distribution), (2) identical shape or morphology, (3) identical chemical composition and crystal structure that are desired between different particles and within individual particles, such as core and surface composition must be the same, and (4) individually dispersed or monodispersed, i.e., no agglomeration. If agglomeration does occur, nanoparticles should be readily redispersible.

Nanoparticles discussed in this chapter include single crystal, polycrystalline, and amorphous particles with all possible morphologies, such as spheres, cubes, and platelets. In general, the characteristic dimension of the particles is not larger than several hundred nanometers, mostly less

than a couple of hundred nanometers. Some other terminologies are commonly used in the literature to describe some specific subgroups of nanoparticles. If the nanoparticles are single crystalline, they are often referred to as nanocrystals. When the characteristic dimension of the nanoparticles is sufficiently small and quantum effects are observed, quantum dots are the common term used to describe such nanoparticles.

3.2. Nanoparticles Through Homogeneous Nucleation

For the formation of nanoparticles by homogeneous nucleation, a supersaturation of growth species must be created. A reduction in temperature of an equilibrium mixture, such as a saturated solution would lead to supersaturating. Formation of metal quantum dots in glass matrix by annealing at elevated temperatures is a good example of this approach. Another method is to generate a supersaturation through *in situ* chemical reactions by converting highly soluble chemicals into less soluble chemicals. For example, semiconductor nanoparticles are commonly produced by pyrolysis of organometallic precursors. Nanoparticles can be synthesized through homogeneous nucleation in three mediums: liquid, gas, and solid; however, the fundamentals of nucleation and subsequent growth processes are essentially the same.

Before discussing the detailed approaches for the synthesis of uniformly sized monodispersed nanoparticles, we will first review the fundamentals of homogeneous nucleation, subsequent growth, and sol–gel processing which are commonly used for the preparation of colloidal dispersions. The various methods for the synthesis of monodispersed uniformly size nanoparticles will be discussed; these include forced hydrolysis, controlled release of cations and anions, vapor phase reactions, and annealing at elevated temperatures.

3.2.1. *Fundamentals of homogeneous nucleation*

When the concentration of a solute in a solvent exceeds its equilibrium solubility or temperature decreases below the phase transformation point, a new phase appears. Let us consider the case homogeneous nucleation of a solid phase from a supersaturated solution as an example. A solution with

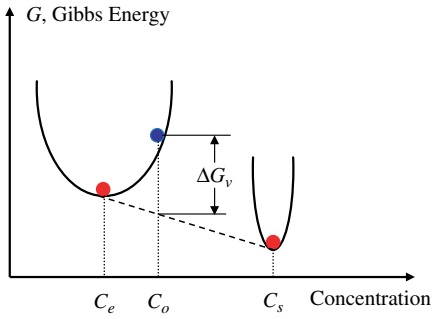

Figure 3.1. Schematic showing the reduction of the overall Gibbs free energy of a supersaturated solution by forming a solid phase and maintaining an equilibrium concentration in the solution.

solute exceeding the solubility or supersaturated possesses a high Gibbs free energy; the overall energy of the system would be reduced by segregating solute from the solution. Figure 3.1 is a schematic showing the reduction of the overall Gibbs free energy of a supersaturated solution by forming a solid phase and maintaining an equilibrium concentration in the solution. This reduction of Gibbs free energy is the driving force for both nucleation and growth. The change of Gibbs free energy per unit volume of the solid phase, $\Delta G_{v,}$ is dependent on the concentration of the solute:

$$\Delta G = \frac{-kT}{\Omega \ln\left(\frac{C}{C_0}\right)} = \frac{-kT}{\Omega \ln(1+\sigma)}, \tag{3.1}$$

where C is the concentration of the solute, C_0 is the equilibrium concentration or solubility, Ω is the atomic volume, and σ is the supersaturation defined by $(C - C_0)/C_0$. Without supersaturation (i.e., $\sigma = 0$), ΔG_v is zero, and no nucleation would occur. When $C > C_0$, ΔG_v is negative and nucleation occurs spontaneously. Assuming a spherical nucleus with a radius of r is formed, the change of Gibbs free energy or volume energy, $\Delta\mu_v$, can be described by:

$$\Delta\mu_v = \left(\frac{4}{3}\right)\pi r^3 \Delta G_v. \tag{3.2}$$

However, this energy reduction is counter balanced by the introduction of surface energy, which accompanied with the formation of new phase. This results in an increase in the surface energy, $\Delta\mu_s$, of the system:

$$\Delta\mu_s = 4\pi r^2\gamma, \tag{3.3}$$

where γ is the surface energy per unit area. The total change of chemical potential for the formation of the nucleus, ΔG, is given by:

$$\Delta G = \Delta\mu_v + \Delta\mu_s = \left(\frac{4}{3}\right)\pi r^3\Delta G_v + 4\pi r^2\gamma. \tag{3.4}$$

Figure 3.2 schematically shows the change of volume free energy, $\Delta\mu_v$, surface free energy, $\Delta\mu_s$, and total free energy, ΔG, as functions of nucleus' radius. From this figure, one can easily see that the newly formed nucleus is stable only when its radius exceeds a critical size, r^*. A nucleus smaller than r^* will dissolve into the solution to reduce the overall free energy, whereas a nucleus larger than r^* is stable and continues to grow bigger. At the critical size $r = r^*$, $d\Delta G/dr = 0$ and the critical size, r^*, and critical energy, ΔG^*, are defined by:

$$r^* = \frac{-2\gamma}{\Delta G_v}, \tag{3.5}$$

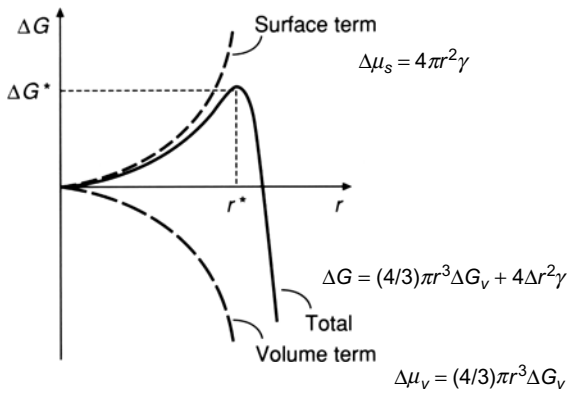

Figure 3.2. Schematic illustrating the change of volume free energy, $\Delta\mu_v$, surface free energy, $\Delta\mu_s$, and total free energy, ΔG, as functions of nucleus' radius.

$$\Delta G^* = \frac{16\pi\gamma}{3(\Delta G_v)^2}, \tag{3.6}$$

ΔG^* is the energy barrier that a nucleation process must overcome and r^* represents the minimum size of a stable spherical nucleus. The above discussion was based on a supersaturated solution; however, all the concepts can be generalized for a supersaturated vapor and a supercooled vapor or liquid.

In the synthesis and preparation of nanoparticles or quantum dots by nucleation from supersaturation solution or vapor, this critical size represents the limit how small nanoparticles can be synthesized. To reduce the critical size and free energy, one need to increase the change of Gibbs free energy, ΔG_v, and reduce the surface energy of the new phase, γ. Equation (3.1) indicated that ΔG_v can be significantly increased by increasing the supersaturation, σ, for a given system. Figure 3.3 compares the critical sizes and critical free energy of three spherical nuclei with different values of supersaturation, which increases with a decreasing temperature. Temperature can also influence surface energy. Surface energy of

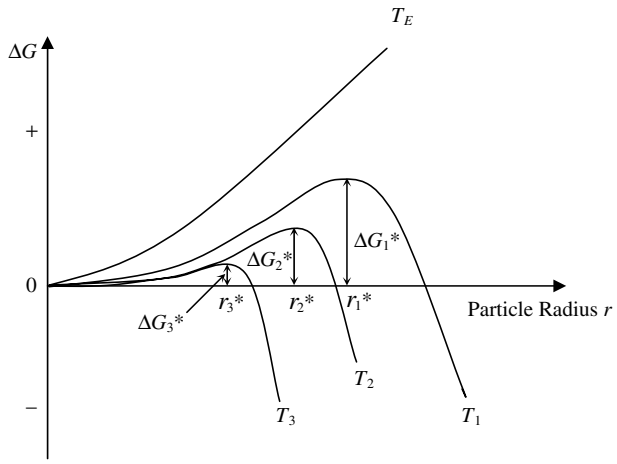

Figure 3.3. The effect of temperature on the critical sizes and critical free energy of three spherical nuclei. Supersaturation increases with a decreasing temperature and surface energy also varies with temperature. $T_E > T_1 > T_2 > T_3$ with T_E being the equilibrium temperature.

the solid nucleus can change more significantly near the roughening temperature. Other possibilities include: (1) use of different solvent, (2) additives in solution, and (3) incorporation of impurities into solid phase, when other requirements are not compromised.

The rate of nucleation per unit volume and per unit time, R_N, is proportional to (1) the probability, P, that a thermodynamic fluctuation of critical free energy, ΔG^*, given by:

$$P = \exp\left(\frac{-\Delta G^*}{kT}\right), \tag{3.7}$$

(2) the number of growth species per unit volume, n, which can be used as nucleation centers (in homogeneous nucleation, it equals to the initial concentration, C_0), and (3) the successful jump frequency of growth species, Γ, from one site to another, which is given by:

$$\Gamma = kT(3\pi\lambda^3\eta), \tag{3.8}$$

where λ is the diameter of the growth species and η is the viscosity of the solution. So the rate of nucleation can be described by:

$$R_N = nP\Gamma = \left\{\frac{C_0 kT}{(3\pi\lambda^3\eta)}\right\}\exp\left(\frac{-\Delta G^*}{kT}\right). \tag{3.9}$$

This equation indicates that high initial concentration or supersaturation (so a large number of nucleation sites), low viscosity, and low critical energy barrier are favoring the formation of a large number of nuclei. For a given concentration of solute, a larger number of nuclei mean smaller sized nuclei.

Figure 3.4 schematically illustrated the processes of nucleation and subsequent growth.[3] When the concentration of solute increases as a function of time, no nucleation would occur even above the equilibrium solubility. The nucleation occurs only when the supersaturation reaches a certain value above the solubility, which corresponds to the energy barrier defined by Eq. (3.6) for the formation of nuclei. After the initial nucleation, the concentration or supersaturation of the growth species decreases and the change of volume Gibbs free energy reduces. When the concentration decreases below this certain concentration, which corresponds to the critical energy, no more nuclei would form, whereas the growth will

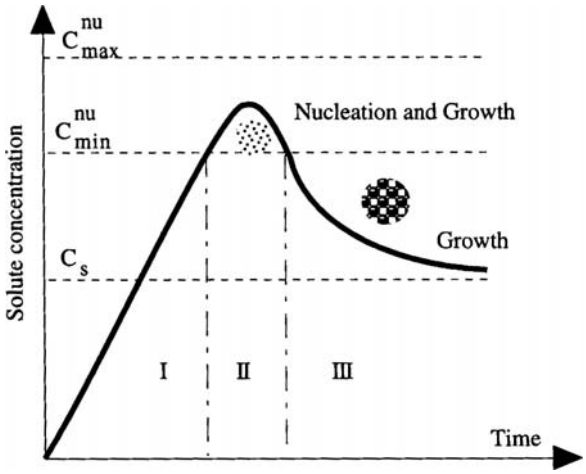

Figure 3.4. Schematic illustrating the processes of nucleation and subsequent growth. [M. Haruta and B. Delmon, *J. Chim. Phys.* **83**, 859 (1986).]

proceed until the concentration of growth species reached the equilibrium concentration or solubility. Figure 3.5 schematically shows, from a slightly different point of view, the relations between the nucleation and growth rates and the concentration of growth species.[3] When the concentration of the growth species increases above the equilibrium concentration, initially there will be no nucleation. However, nucleation occurs when the concentration reaches the minimum saturation required to generate the critical free energy, and the nucleation rate increases very rapidly as the concentration increases further. Although growth process cannot proceed when there is no nucleus, growth rate is above zero for a concentration above its equilibrium solubility. Once nuclei are formed, growth occurs simultaneously. Above the minimum concentration, nucleation and growth are inseparable processes; however, these two processes proceed in different speeds.

For the synthesis of nanoparticles with uniform size distribution, it will be the best if all nuclei form at the same time with the same size. In this case, all the nuclei are likely to have the same or similar size, since they are formed under the same conditions. In addition, all the nuclei will have the same subsequent growth. Consequently, monosized

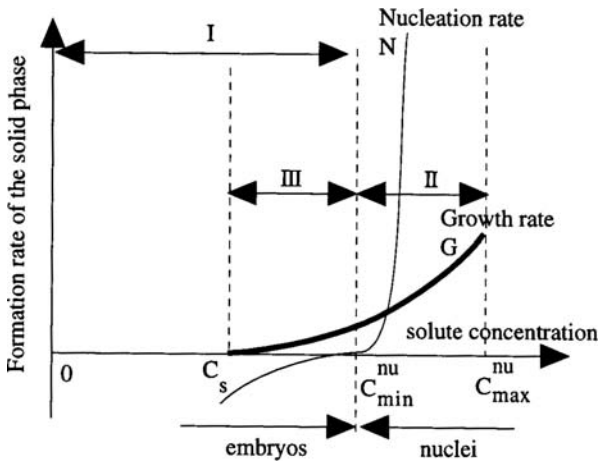

Figure 3.5. Schematic showing, from a slightly different point of view, the relations between the nucleation and growth rates and the concentration of growth species. [M. Haruta and B. Delmon, *J. Chim. Phys.* **83**, 859 (1986).]

nanoparticles can be obtained. So it is obvious that it is highly desirable to have nucleation occur in a very short period of time. In practice, to achieve a sharp nucleation, the concentration of the growth species is increased abruptly to a very high supersaturation and then is quickly brought below the minimum concentration for nucleation. Below this concentration, no more new nucleus forms, whereas the existing nuclei continue to grow until the concentration of the growth species reduces to the equilibrium concentration. The size distribution of nanoparticles can be further altered in the subsequent growth process. The size distribution of initial nuclei may increase or decrease depending on the kinetics of the subsequent growth process. The formation of uniformly sized nanoparticles can be achieved if the growth process is appropriately controlled.

3.2.2. *Subsequent growth of nuclei*

The size distribution of nanoparticles is dependent on the subsequent growth process of the nuclei. The growth process of the nuclei involves multi-steps and the major steps are (1) generation of growth species, (2) diffusion of the growth species from bulk to the growth surface,

(3) adsorption of the growth species onto the growth surface, and (4) surface growth through irreversible incorporation of growth species onto the solid surface. These steps can be further grouped into two processes. Supplying the growth species to the growth surface is termed as diffusion, which includes the generation, diffusion, and adsorption of growth species onto the growth surface, whereas incorporation of growth species adsorbed on the growth surface into solid structure is denoted as growth. A diffusion-limited growth would result a different size distribution of nanoparticles as compared with that by growth-limited process.

3.2.2.1. *Growth controlled by diffusion*

When the concentration of growth species reduces below the minimum concentration for nucleation, nucleation stops, whereas the growth continues. If the growth process is controlled by the diffusion of growth species from the bulk solution to the particle surface, the growth rate is given by[4]:

$$\frac{dr}{dt} = \frac{D(C - C_s)V_m}{r}, \tag{3.10}$$

where r is the radius of spherical nucleus, D is the diffusion coefficient of the growth species, C is the bulk concentration, C_s is the concentration on the surface of solid particles, and V_m is the molar volume of the nuclei as illustrated in Fig. 3.6. By solving this differential equation and assuming the initial size of nucleus, r_0, and the change of bulk concentration negligible, we have:

$$r^2 = 2D(C - C_s)V_m t + {r_0}^2 \tag{3.11}$$

or

$$r^2 = k_D t + {r_0}^2, \tag{3.12}$$

where $k_D = 2D(C - C_s)V_m$. For two particles with initial radius difference, δr_0, the radius difference, δr, decreases as time increases or particles grow bigger, according to:

$$\delta r = \frac{r_0 \delta r_0}{r}. \tag{3.13}$$

Combining with Eq. (3.12), we have:

$$\delta r = \frac{r_0 \delta r_0}{\left(k_D t + r_0^{\,2}\right)^{\frac{1}{2}}}. \tag{3.14}$$

Both Eqs. (3.13) and (3.14) indicate that the radius difference decreases with increase of nuclear radius and prolonged growth time. The diffusion-controlled growth promotes the formation of uniformly size particles.

3.2.2.2. *Growth controlled by surface process*

When the diffusion of growth species from the bulk to the growth surface is sufficiently rapid, i.e., the concentration on the surface is the same as that in the bulk as illustrated by a dash line also in Fig. 3.6, the growth rate is controlled by the surface process. There are two mechanisms for the surface processes: mononuclear growth and polynuclear growth. For the mononuclear growth, the growth proceeds layer by layer; the growth species are incorporated into one layer and proceeds to another layer only after the growth of the previous layer is complete. There is a sufficient time for the growth species to diffuse on the surface. The growth rate is thus proportional to the surface area[4]:

$$\frac{dr}{dt} = k_m(C) r^2, \tag{3.15}$$

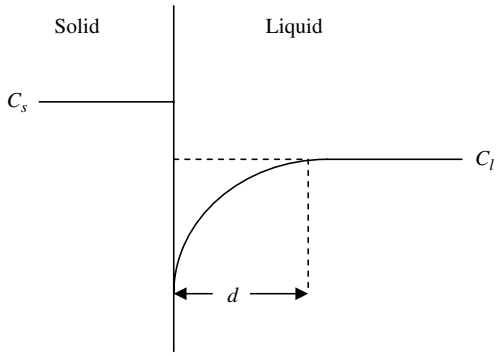

Figure 3.6. Schematic diagram of the concentration profile of an alloy component or impurity distribution across the solid/liquid interface, showing the formation of a depletion boundary layer in the liquid phase.

where $k_m(C)$ is a proportionality constant, dependent on the concentration of growth species. The growth rate is given by solving the above equation:

$$\frac{1}{r} = \frac{1}{r_0} - k_m t. \tag{3.16}$$

The radius difference increases with an increasing radius of the nuclei:

$$\delta r = \frac{r^2 \delta r_0}{{r_0}^2}. \tag{3.17}$$

Substituting Eq. (3.16) into Eq. (3.17) yields:

$$\delta r = \frac{\delta r_0}{(1 - k_m r_0 t)^2}, \tag{3.18}$$

where $k_m t r_0 < 1$. This boundary condition is derived from Eq. (3.16), and means that the radius if nucleus is not infinite large, i.e., $r < \infty$. Equation (3.18) shows that the radius difference increases with a prolonged growth time. Obviously, this growth mechanism does not favor the synthesis of monosized particles.

During polynuclear growth, which occurs when the surface concentration is very high, surface process is so fast that second layer growth proceeds before the first layer growth is complete. The growth rate of particles is independent of particle size or time,[5] i.e., the growth rate is constant:

$$\frac{dr}{dt} = k_p, \tag{3.19}$$

where k_p is a constant only dependent on temperature. Hence the particles grow linearly with time:

$$r = k_p t + r_0. \tag{3.20}$$

The relative radius difference remains constant regardless the growth time and the absolute particle size:

$$\delta r = \delta r_0. \tag{3.21}$$

It is worthy noting that although the absolute radius difference remains unchanged, the relative radius difference would be inversely proportional to the particle radius and the growth time. As particles get bigger, the radius difference become smaller; so this growth mechanism also favors the synthesis of monosized particles.

Figures 3.7 and 3.8 schematically illustrate the radius difference as functions of particle size and growth time for all three mechanisms of subsequent growth discussed above. It is obvious that a diffusion-controlled growth mechanism is required for the synthesis of monosized particles by homogeneous nucleation. Williams *et al*.[5] suggested that the growth of nanoparticles involve all three mechanisms. When the nuclei are small, monolayer growth mechanism may dominate, polynuclear growth may become predominant as the nuclei become bigger. Diffusion is predominant for the growth of relatively large particles. Of course, this would only be the case when no other procedures or measures were applied to prevent certain growth mechanisms. Different growth mechanisms can become predominant when favorable growth conditions are established. For example, when the supply of growth species is very slow due to a slow chemical reaction, the growth of nuclei would most likely be predominant by the diffusion-controlled process.

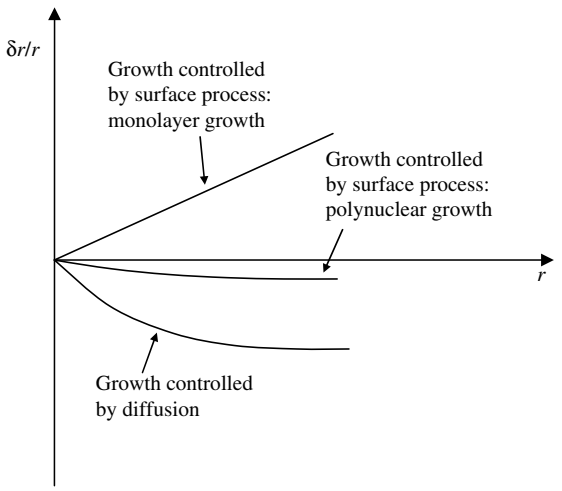

Figures 3.7. Schematic illustrating the radius difference as functions of particle size for all three mechanisms of subsequent growth.

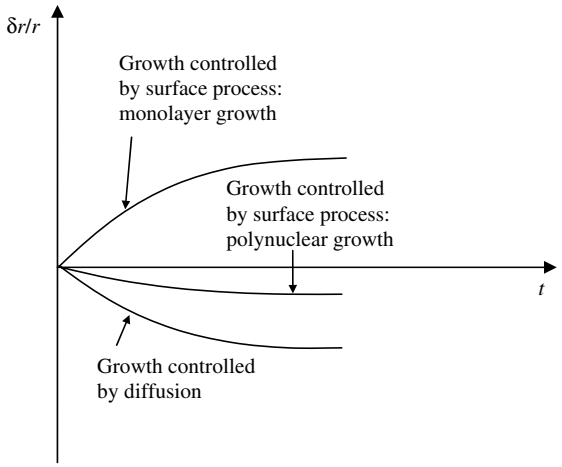

Figure 3.8. Schematic illustrating the radius difference as functions of growth time for all three mechanisms of subsequent growth.

For the formation of monosized nanoparticles, diffusion-limited growth is desired. There are several ways to achieve diffusion-limited growth. For example, when the concentration of growth species is kept extremely low, diffusion distance would be very large and consequently diffusion could become the limiting step. Increasing the viscosity of solution is another possibility. Introduction of a diffusion barrier such as a monolayer on the surface of a growing particle is yet another approach. Controlled supply of growth species offers another method to manipulate the growth process. When growth species is generated through chemical reactions, the rate of reaction can be manipulated through the control of the concentration of by-product, reactant, and catalyst.

In the following sections, we will discuss the synthesis of metal, semiconductor, and oxide (including hydroxide) nanoparticles separately for the sake of clarity. First, we will focus our discussion on the synthesis of various types of nanoparticles through solution processes. Formation of nanoparticles dispersed in a solvent is the most common approach and offers several advantages, which include:

(1) Easiness of stabilization of nanoparticles from agglomeration
(2) Easiness of extraction of nanoparticles from solvent

(3) Easiness for surface modification and application
(4) Easiness of processing control, and
(5) Mass production.

3.2.3. *Synthesis of metallic nanoparticles*

Reduction of metal complexes in dilute solutions is the general method in the synthesis of metal colloidal dispersions, and a variety of methods have been developed to initiate and control the reduction reactions.[6–10] The formation of monosized metallic nanoparticles is achieved in most cases by a combination of a low concentration of solute and polymeric monolayer adhered onto the growth surfaces. Both a low concentration and a polymeric monolayer would hinder the diffusion of growth species from the surrounding solution to the growth surfaces, so that the diffusion process is likely to be the rate limiting step of subsequent growth of initial nuclei, resulting in the formation of uniformly sized nanoparticles.

In the synthesis of metallic nanoparticles, or more specifically speaking, metallic colloidal dispersion, various types of precursors, reduction reagents, other chemicals, and methods were used to promote or control the reduction reactions, the initial nucleation and the subsequent growth of initial nuclei. Table 3.1 briefly summarizes the precursors, reduction reagents, and polymeric stabilizers commonly used in the production of metallic colloidal dispersions. The precursors include: elemental metals, inorganic salts, and metal complexes, such as, Ni, Co, $HAuCl_4$, H_2PtCl_6, $RhCl_3$, and $PdCl_2$. Reduction reagents includes: sodium citrate, hydrogen peroxide, hydroxylamine hydrochloride, citric acid, carbon monoxide, phosphorus, hydrogen, formaldehyde, aqueous methanol, sodium carbonate, and sodium hydroxide. Examples of polymeric stabilizers include polyvinyl alcohol (PVA) and sodium polyacrylate.

Colloidal gold has been studied extensively for a long time. In 1857 Faraday published a comprehensive study on the preparation and properties of colloidal gold.[11] A variety of methods have been developed for the synthesis of gold nanoparticles, and among them, sodium citrate reduction of chlorauric acid at 100°C was developed more than 50 years ago[12] and remains the most commonly used method. The classical (or standard) experimental conditions are as follows. Chlorauric acid dissolves into

Table 3.1. Summary of precursors, reduction reagents and polymer stabilizers.

Precursors	Formula
Metal anode	Pd, Ni, Co
Palladium chloride	$PdCl_2$
Hydrogen hexachloroplatinate IV	H_2PtCl_6
Potassium tetrachloroplatinate II	K_2PtCl_4
Silver nitrate	$AgNO_3$
Silver tetraoxylchlorate	$AgClO_4$
Chloroauric acid	$HAuCl_4$
Rhodium chloride	$RhCl_3$
Reduction reagents	
Hydrogen	H_2
Sodium citrate	$Na_3C_6H_5O_7$
Hydroxylamine hydrochloride	$NH_4OH + HCl$
Citric acid	$C_6H_8O_7$
Carbon monoxide	CO
Phosphorus in ether	P
Methanol	CH_3OH
Hydrogen peroxide	H_2O_2
Sodium carbonate	Na_2CO_3
Sodium hydroxide	NaOH
Formaldehyde	HCHO
Sodium tetrahydroborate	$NaBH_4$
Ammonium ions	NH_4^-
Polymer stabilizers	
Poly(vinylpyrrolidone), PVP	
Polyvinylalcohol, PVA	
Polyethyleneimine	
Sodium polyphosphate	
Sodium polyacrylate	
Tetraalkylammonium halogenides	

water to making 20 ml very dilute solution of ~2.5×10^{-4} M. Then 1 ml 0.5% sodium citrate is added into the boiling solution. The mixture is kept at 100°C till color changes, while maintaining the overall volume of the solution by adding water. Such prepared colloidal sol has excellent stability and uniform particle size of ~20 nm in diameter. It has been

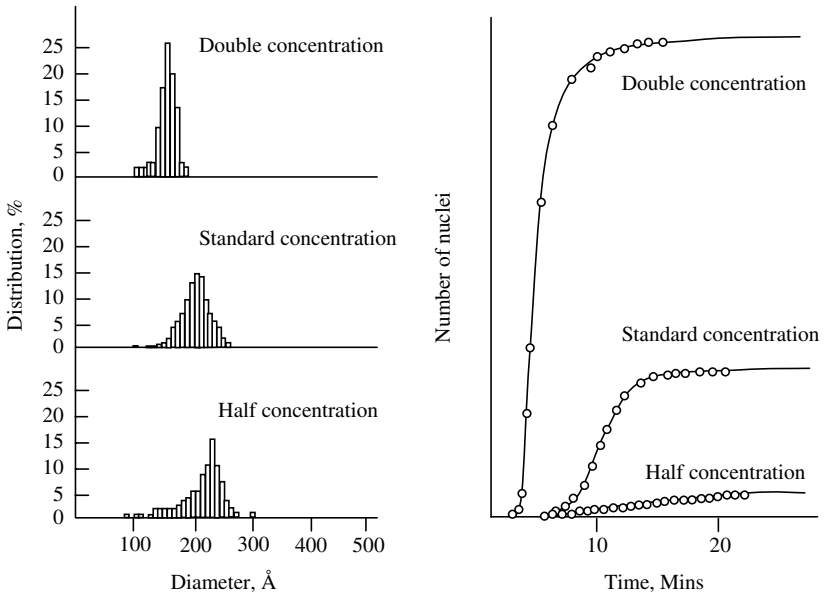

Figure 3.9. (left) Particle size distribution curves of gold sol prepared at different concentrations (right) Nucleation rate curves for gold sols prepared at different concentrations. [J. Turkevich, *Gold Bull*. **18**, 86 (1985).]

demonstrated that a large number of initial nuclei formed in the nucleation stage would result in a larger number of nanoparticles with smaller size and narrower size distribution. Figure 3.9 compares the size and size distribution of gold nanoparticles and the nucleation rates when the colloidal gold was prepared at different concentrations.[13]

Hirai and coworkers[14,15] prepared a colloidal dispersion of rhodium by refluxing a solution of rhodium chloride and PVA in a mixture of methanol and water at 79°C. The volume ratio of methanol to water was 1:1. Refluxing was carried out in argon or air for 0.2 to 16 h. In this process, methanol was used as a reduction reagent and the reduction reaction was straightforward:

$$RhCl_3 + \frac{3}{2}CH_3O_3 \rightarrow Rh + \frac{3}{2}HCHO + 3HCl. \tag{3.22}$$

PVA was used as a polymer stabilizer and also served as a diffusion barrier. Rh nanoparticles prepared were found to have mean diameters

ranging from 0.8 to 4 nm. However, a bimodal size distribution was found, with large particles of 4 nm and small ones of 0.8 nm. Increasing refluxing time was found to result in a decrease of small particles and an increase of large particles, which was attributed to Ostwald ripening.

Henglein *et al*.[16] studied and compared three different methods for the preparation of Pt nanoparticles: radiolysis, hydrogen reduction, and citrate reduction. The γ-rays of ^{60}Co was used to generate hydrated electrons, hydrogen atoms, and 1-hydroxylmethyl radicals. These radicals would subsequently reduce Pt^{2+} in K_2PtCl_4 to the zero-valence state, which formed Pt particles with a mean diameter of 1.8 nm. Citrate reduction of $PtCl_6^{2-}$ is also known as Turkevich method,[12,17,18] which was initially developed for the synthesis of uniformly sized gold nanoparticles. In this method, H_2PtCl_6 was mixed with sodium citrate and boiled for 1 h, yielded Pt particles of 2.5 nm in diameter.

Hydrogen reduction of K_2PtCl_4 and $PdCl_2$ was developed by Rampino and Nord[19] and PVA was used to stabilize both Pt and Pd particles in the experiments. In this method, precursors in dilute aqueous solution were first hydrolyzed to form hydroxides prior to hydrogen reduction. For Pd, sodium carbonate was used as a catalyst to promote the hydrolysis reaction, whereas for Pt, sodium hydroxide was required to ensure the hydrolysis reaction. For palladium, the following reduction reactions were proposed:

$$PdCl_2 + Na_2CO_3 + 2H_2O \rightarrow Pd(OH)_2 + H_2CO_3 + 2Na^+ + 2Cl^-, \quad (3.23)$$

$$Pd(OH)_2 + H_2 \rightarrow Pd + 2H_2O. \quad (3.24)$$

Similar reactions were proposed for the synthesis of Pt nanoparticles. When no catalyst was used, during aging prior to the introduction of hydrogen gas, the Pt precursor complexes could be converted to a large extent into aquated complexes within a few hours at ambient temperature[20]:

$$PtCl_4^{2-} + H_2O \rightarrow Pd(H_2O)Cl_3^- + Cl^-, \quad (3.25)$$

$$Pt(H_2O)Cl_3^- + H_2O \rightarrow Pt(H_2O)_2Cl_2 + Cl^-. \quad (3.26)$$

The aquated complexes were then reduced by hydrogen. It was found that the polymeric stabilizer, either sodium polyacrylate or polyphosphate, had a strong influence on the rate of the reduction reaction. This indicates that the polymeric stabilizer may exert catalytic influences on reduction, in addition to their stabilization and diffusion barrier roles. Such prepared Pt particles have a mean diameter of 7.0 nm.

Various methods are developed for the formation of silver nanoparticles. For example synthesis of Ag nanoparticles can be achieved by the UV illumination of aqueous solutions containing $AgClO_4$, acetone, 2-propanol and various polymer stabilizers.[31] UV illumination generates ketyl radicals via excitation of acetone and subsequent hydrogen atom abstraction from 2-propanol:

$$CH_3COCH_3^* + (CH_3)_2CHOH \rightarrow 2(CH_3)_2(OH)C^{\bullet}. \tag{3.27}$$

The ketyl radical may further undergo protolytic dissociation reaction:

$$(CH_3)_2(OH)C^{\bullet} \Leftrightarrow (CH_3)_2OC^{\bullet -} + H^+. \tag{3.28}$$

Both the ketyl radical and radical anions react with and reduce silver ions to silver atoms:

$$(CH_3)_2(OH)C^{\bullet} + Ag^+ \rightarrow (CH_3)_2CO + Ag + H^+, \tag{3.29}$$

$$(CH_3)_2OC^{\bullet -} + Ag^+ \rightarrow (CH_3)_2CO + Ag. \tag{3.30}$$

Both reactions have a rather low reaction rate, and thus favor the production of monosized silver nanoparticles. With the presence of polyethyleneimine as polymer stabilizer, silver nanoparticles formed using the above photochemical reduction process have a mean size of 7 nm with a narrow size distribution.

Amorphous silver nanoparticles of ~20 nm size were prepared by sonochemical reduction of an aqueous silver nitrate solution at a temperature of 10°C, in an atmosphere of argon and hydrogen.[21] The reaction was explained as follows. The ultrasound resulted in decomposition of

water into hydrogen and hydroxyl radicals. Hydrogen radicals would reduce silver ions into silver atoms, which subsequently nucleate and grow to silver nanoclusters. Some hydroxyl radicals would combine to form an oxidant, hydrogen peroxide, which may oxidize silver nanoclusters to silver oxide, and the addition of hydrogen gas was to remove the hydrogen peroxides from the solution so as to prevent the oxidation of silver nanoparticles.[22]

Metallic nanoparticles can also be prepared by an electrochemical deposition method.[23,24] This synthesis employs a simple electrochemical cell containing only a metal anode and a metal or glassy carbon cathode. The electrolyte consists of organic solutions of tetraalkyammonium halogenides, which also serve as stabilizers for the produced metal nanoparticles. Upon application of an electric field, the anode undergoes oxidative dissolution forming metal ions, which would migrate toward the cathode. The reduction of metal ions by ammonium ions leads to the nucleation and subsequent growth of metallic nanoparticles in the solutions. With this method, nanoparticles of Pd, Ni, and Co with diameters ranging from 1.4 to 4.8 nm were produced. Furthermore, it was found that the current density has an appreciable influence on the size of metallic particles; increasing the current density results in a reduced particle size.[23]

3.2.3.1. *Influences of reduction reagents*

The size and size distribution of metallic colloids varied significantly with the types of reduction reagents used in the synthesis. In general, a strong reduction reaction promotes a fast reaction rate and favors the formation of smaller nanoparticles.[25,26] A weak reduction reagent induces a slow reaction rate and favors relatively larger particles. However, a slow reaction may result in either wider or narrower size distribution. If the slow reaction leads to continuous formation of new nuclei or secondary nuclei, a wide size distribution would be obtained. On the other hand, if no further nucleation or secondary nucleation occurs, a slow reduction reaction would lead to diffusion-limited growth, since the growth of the nuclei would be controlled by the availability of the zerovalent atoms. Consequently, a narrow size distribution would be obtained.

Table 3.2. Comparison of average sizes of Au nanoparticles synthesized using various reduction reagents, all in nanometer.[27]

Reduction reagents	436 nm*	546 nm*	XRD#	SEM
Sodium citrate	29.1	28.6	17.5	17.6 ± 0.6
Hydrogen peroxide	25.3	23.1	15.1	15.7 ± 1.1
	31.0	31.3	18.7	19.7 ± 2.6
Hydroxylamine hydrochloride			37.8	22.8 ± 4.2
Citric acid	23.5	22.8		12.5 ± 0.6
Carbon monoxide	9.1	7.4	9.0	5.0 ± 0.5
	15.3	15.3	9.8	7.5 ± 0.4
	18.9	18.3	13.1	12.2 ± 0.5
Phosphorus			13.9	8.1 ± 0.5
			21.0	15.5 ± 1.7
			29.6	25.6 ± 2.6
			36.9	35.8 ± 9.7

* The particles sizes are determined using light scattering with the indicated wavelengths.

The particle sizes are determined based on X-ray diffraction line broadening.

The influences of various reduction reagents on the size and size distribution of gold nanoparticles are summarized in Table 3.2.[27] Using the same reduction reagent, nanoparticle size can be varied by changing the synthesis conditions. In addition, it was found that the reduction reagents have noticeable influences on the morphology of the gold colloidal particles. Figure 3.10 shows electron micrographs of gold nanoparticles prepared with sodium citrate (a) and citric acid (b) as reduction reagents, respectively, under otherwise similar synthesis conditions.[27] Gold particles with spherical shape were obtained using sodium citrate or hydrogen peroxide as reduction reagents, whereas faceted gold particles were formed when hydroxylamine hydrochloride (cubical with {100} facets) and citric acid (trigons or very thin platelets of trigonal symmetry with {111} facets) were used as reduction reagents. Furthermore, concentration of the reduction reagents and pH value of the reagents were all noticeable influences on the morphology of the grown gold nanoparticles. For example, lowering the pH value caused the {111} facets to develop at the expense of the {100} facets.

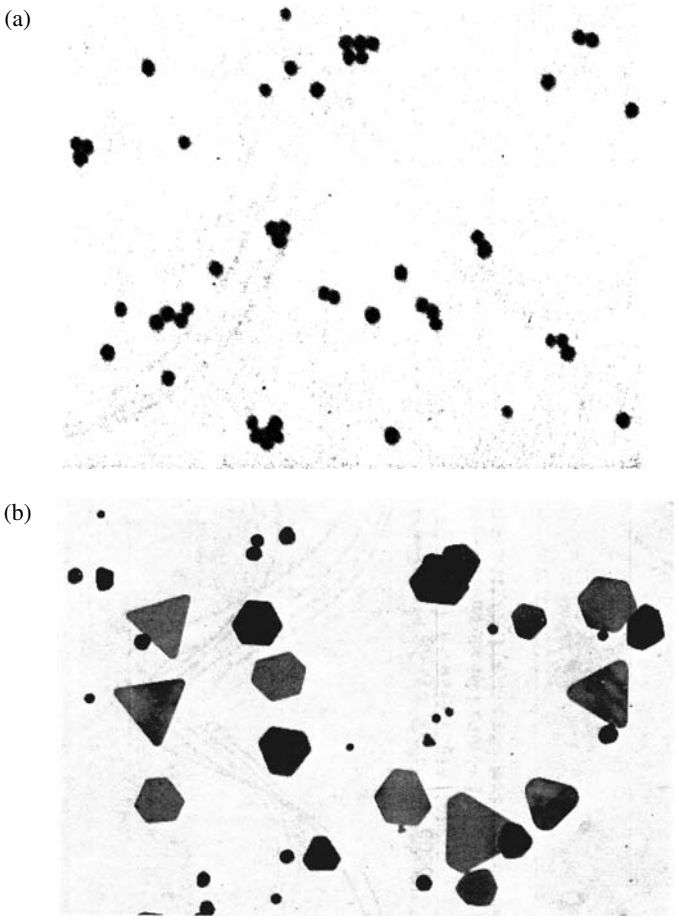

Figure 3.10. SEM micrographs of gold nanoparticles prepared with sodium citrate (a) and citric acid (b) as reduction reagents, respectively, under otherwise similar synthesis conditions. [W.O. Miligan and R.H. Morriss, *J. Am. Chem. Soc*. **86**, 3461 (1964).]

In preparation of transition metallic colloids, Reetz and Maase[28] found that the size of metallic colloids is strongly dependent on how strong a reduction reagent is, and stronger reducing reagents lead to smaller nanoparticles. For example, for the synthesis of Pd colloids from lead nitrate in THF, the particle size decreases in the following order:

$$r_{\text{pivalate}} \approx r_{\text{acetate}} > r_{\text{glycolate}} \gg r_{\text{dichloroacetate}}. \tag{3.31}$$

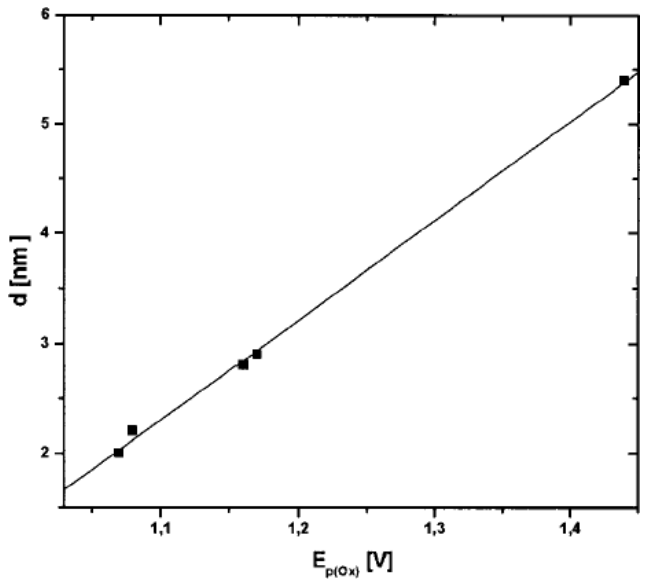

Figure 3.11. The particle size of Pd colloids as a function of peak potentials of reduction reagent, carboxylates, in which smaller peak potentials mean stronger reduction reagents. [M.T. Reetz and M. Maase, *Adv. Mater.* **11**, 773 (1999).]

Figure 3.11 shows the particle size of Pd colloids as a function of peak potentials of reduction reagent, carboxylates, in which smaller peak potentials mean stronger reduction reagents.[28] Such an influence may be explained by the fact that stronger reduction reagent would generate an abrupt surge of the concentration of growth species, resulting in a very high supersaturation. Consequently, a large number of initial nuclei would form. For a given concentration of metal precursors, the formation of a larger number of nuclei would result in a smaller size of the grown nanoparticles.

3.2.3.2. *Influences by other factors*

In addition to the control by reduction reagents, the reduction reaction rate or the supply of the growth species can be influenced by other factors. For example, in the synthesis of Pt nanoparticles using an aqueous methanol

reduction of H_2PtCl_6, Duff *et al.*[29] found that a high concentration of chloride ions present in the reaction mixture promoted monodispersity and near-spherical particle shape of the metallic colloids, favoring smoother and rounder surfaces, at otherwise the similar conditions. Such an influence could be understood from the two-step reduction reactions:

$$PtCl_6^{2-} + CH_3OH \rightarrow PtCl_4^{2-} + HCHO + 2H^+ + 2Cl^-, \tag{3.32}$$

$$PtCl_4^{2-} + CH_3OH \rightarrow Pt + HCHO + 2H^+ + 4Cl^-. \tag{3.33}$$

An increased concentration of chloride ions would favor slow reaction rates. Consequently, the supply of the growth species, i.e., zerovalent Pt atom, would be slow and, thus, favors diffusion-limited growth of initial Pt nuclei. Further, increasing the amount of polymer in the reaction mixture was found to increase the sphericity of the particles. It can be easily understood by considering the fact that increased amount of polymer produce steric resistance for the diffusion and consequently result in a diffusion-controlled growth, which favors the formation of spherical particles.

A decreased reduction rate can also be achieved using a low concentration of reactant, which is illustrated by the following example. Nanosized silver particles were synthesized by reduction of silver nitrate using formaldehyde in aqueous solution.[30] It was found that the quantity of reducing agent had negligible effects on the particle size distribution; however, if only formaldehyde was used, the reaction rate would be too slow at room temperature due to low pH. Alkaline solution consisting of NaOH and/or Na_2CO_3 was used to promote the over reaction rate. The reaction between silver ions and reducing agent can be written as:

$$2Ag^+ + HCHO + 3OH^- \rightarrow 2Ag + HCOO^- + 2H_2O, \tag{3.34}$$

$$Ag^+ + HCHO + OH^- \rightarrow Ag + HCOOH + \frac{1}{2}H_2. \tag{3.35}$$

The following reaction mechanism was proposed. First hydroxyl ions may undergo a nucleophilic addition reaction to formaldehyde producing

hydride and formate ions, and then the hydride ions reduce silver ions to silver atoms.

When only NaOH was used, a higher pH was found to favor for higher reduction rate and result in the formation of large silver precipitates, which settle at the bottom of solution. When a weak base of sodium carbonate was added to partially substitute NaOH, stable silver colloidal dispersions were obtained. The addition or substitution of sodium carbonate is to control the release of hydroxyl ions only when the pH became lower than certain value according to the following reaction:

$$Na_2CO_3 + 2H_2O \Leftrightarrow 2Na^+ + 2OH^- + H_2CO_3. \quad (3.36)$$

The concentration of hydroxyl ions would determine the rate of reactions 3.34 and 3.35, so as to controlled the production of silver atoms. Figure 3.12 shows the effect of the quantity of sodium carbonate on the average size of silver particles and the standard deviation of size

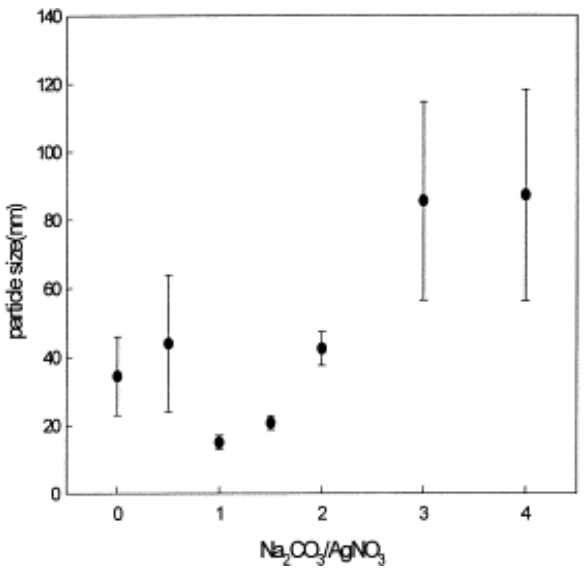

Figure 3.12. Effect of $[Na_2CO_3]/[AgNO_3]$ ratio on silver average size and its standard deviation (other conditions: $[AgNO_3] = 0.005$ M, $[HCHO]/[AgNO_3] = 4$, $[NaOH]/[AgNO_3] = 1$, $PVP/[AgNO_3] = 9.27$). [K. Chou and C. Ren, *Mater. Chem. Phys*. **64**, 241 (2000).]

distribution.[30] Well-dispersed crystalline silver particles of 7–20 nm in size and with spherical shape were obtained with a $Na_2CO_3/AgNO_3$ ratio ranging from 1 to 1.5. More Na_2CO_3 resulted in a higher pH or a higher concentration of hydroxyl ions, which would promote the reduction rates. A higher concentration of Na_2CO_3 would increase the concentration of hydroxyl ions and, thus, promote the reduction rate, resulting in the production of large quantity of growth species and shift the growth away from diffusion limiting process. It should also be noted that during the synthesis, polyvinyl-pyrrolidone (PVP) or polyvinyl alcohol (PVA) was used to stabilize the grown silver nanoparticles. As discussed before, the presence of the polymeric layer would also serve as a diffusion barrier, so that promotes the diffusion-limited growth, favoring a narrow size distribution.

3.2.3.3. *Influences of polymer stabilizer*

Henglein[31] systematically studied the influences of various polymer stabilizers on the formation of silver colloidal dispersions. The polymer stabilizers studied are polyethyleneimine, sodium polyphosphate, sodium polyacrylate, and poly(vinylpyrrolidone). Although polymer stabilizers are introduced primarily to form a monolayer on the surface of nanoparticles so as to prevent agglomeration of nanoparticles, the presence of such polymer stabilizers during the formation of nanoparticles can have various influences on the growth process of nanoparticles. Interaction between the surface of a solid particle and polymer stabilizer may vary significantly depending on the surface chemistry of the solid, the polymer, solvent, and temperature. A strong adsorption of polymer stabilizers would occupy the growth sites and thus reduce the growth rate of nanoparticles. A full coverage of polymer stabilizer would also hinder the diffusion of growth species from the surrounding solution to the surface of growing particle.

Polymer stabilizers may also interact with solute, catalyst, or solvent, and thus directly contribute to reaction. For example, Chou and Ren[30] reported that PVP is actually a weak acid and capable of combining with hydroxyl ions. As a result, the effective quantity of PVP as a stabilizer would be smaller than that was added. Polymer stabilizers have also been

found to have catalytic effect on reduction reactions.[16] Furthermore, the pH of the solution would increase with an increasing concentration of PVP.

Ahmadi *et al*.[32] studied the influences of polymer stabilizer (also referred to as capping material), sodium polyacrylate, on the shape of colloidal platinum nanoparticles. Their results demonstrated that under the same experimental conditions and using the same polymer stabilizer, changing the ratio of the concentration of the capping material to that of Pt ions from 1:1 to 5:1 produced different shapes of Pt nanoparticles, with cubic particles in corresponding to a ratio of 1:1 and tetrahedral particles to a 5:1 ratio. Obviously the different concentration ratio of capping material has determining influences on the growth rate of {111} and {100} facets of Pt nuclei. Figure 3.13 shows the different morphologies of Pt nanoparticles.[32]

It should also be noted that although polymer stabilizers play a very important role in the synthesis of metal nanoparticles, metal nanoparticles

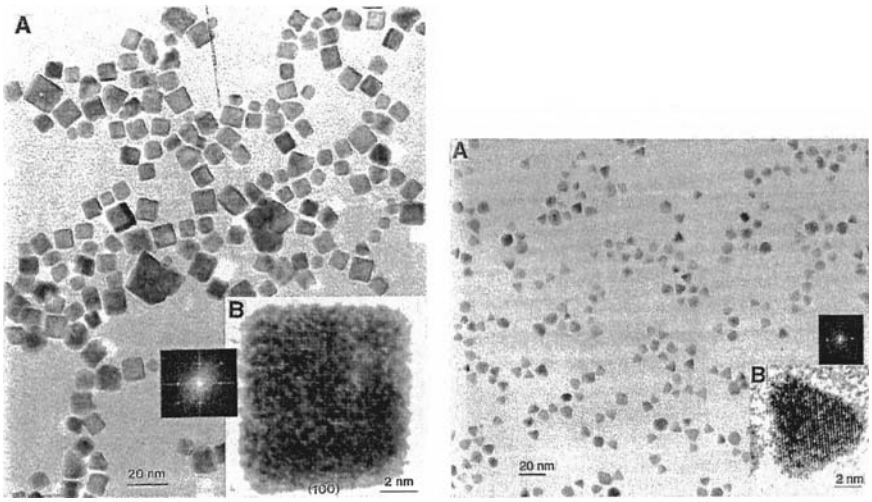

Figure 3.13. Pt nanoparticles synthesized in colloidal solution and having different shapes (11 nm cubes on the left and ~7 nm tetrahedrons on the right). The potential use of these nanoparticles for different types of catalyses drives our research interest in these particles. [T.S. Ahmadi, Z.L. Wang, T.C. Green, A. Henglein, and M.A. El-Sayed, *Science* **272**, 1924 (1996).]

can be prepared without using any polymer stabilizers.[21,33] Yin *et al*.[33] prepared silver nanoparticles through tollens process using a commercially available set of solution.[34] Without adding any stabilizing reagent, the as-synthesized aqueous dispersion of silver nanoparticles of 20–30 nm in size was found to be stable for at least one year. The dispersion is likely to be stabilized by electrostatic stabilization mechanism. However, the particle size is sensitively dependent on the synthesis temperature. A small variation of temperature would result in a significant change of diameters of metal nanoparticles. Figure 3.14 compares the silver nanoparticles synthesized under different temperatures.[33]

Furthermore, nanoparticles of metals or metal alloys were prepared through seeding nucleation. For example, Toneguzzo *et al*.[35] reported that polymetallic fine particles Co_xNi_{1-x} and $Fe_z[Co_xNi_{1-x}]_{1-z}$ were synthesized by precipitation from metallic precursors dissolved in 1, 2-propanediol with an optimized amount of sodium hydroxide. The precursors used were tetrahydrated cobalt (II), nickel (II) acetate, and tetrahydrated iron (II) chloride. The particle formation was initiated by adding a small amount of a solution of K_2PtCl_4 or $AgNO_3$ in 1, 2-ethanediol. Pt or Ag is believed to act as nucleation agent. An increased concentration of Pt or Ag relative to the concentration of Co, Ni, and Fe resulted in a reduced mean particle size, implying an increased number of particles.

Considerable research attention has been paid to the preparation of nanomaterials with high magnetic moment due to their potential biomedical applications including bioseparation, biosensing, magnetic imaging, drug delivery and magnetic fluid hyperthermia.[36] Homogeneous nanomaterials such as monodisperse soft ferromagnetic nanoparticles can fulfill this demand excellently. Nanoparticles for magnetic and biomagnetic applications include particles of metals, metal alloys, oxides, and metal-oxide core–shell structures.

Cobalt has high magnetic moment (160 emu/g or 1422 emu/cc) and is magnetically soft, which means it can be magnetized by weaker magnetic field and lower residual magnetism compared to hard magnetic material. Co hollow nanoparallelepipeds can be synthesized via hermolysis of CoO solid nanoparallelepipeds with FCC structure in oleylamine.[37] The fast diffusion of CoO toward outside leads to a hollow structure and CoO will be reduced by oleylamine later. The diameter of the voids is about 7 nm.

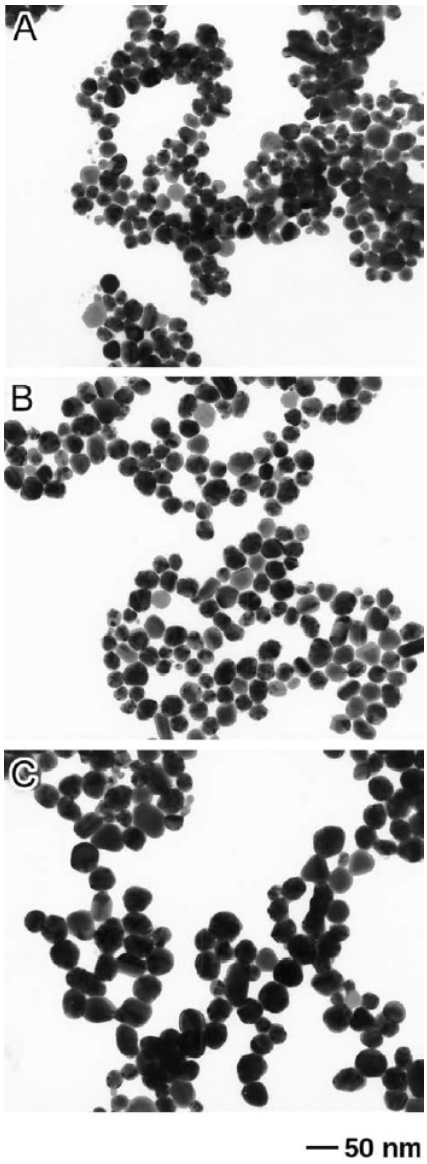

Figure 3.14. TEM images of silver nanoparticles that were obtained as final products when the reactions were carried out under nitrogen at (A) 27, (B) 30, and (C) 35°C, respectively. The mean size of these silver nanoparticles changed from ~20, to ~30 and ~40 nm when the temperature was raised. [Y. Yin, Z. Li, Z. Zhong, B. Gates, Y. Xia, and S. Venkateswaran, *J. Mater. Chem*. **12**, 522 (2002).]

This hollow structure with large surface area leads to an unusual paramagnetic material. Figure 3.15 shows the evolution of the morphology of fcc Co hollow nanoparallelepipeds with time (a→d) when a slurry of fcc CoO solid nanoparallelepipeds in oleylamine are heated at 290°C for 2 h

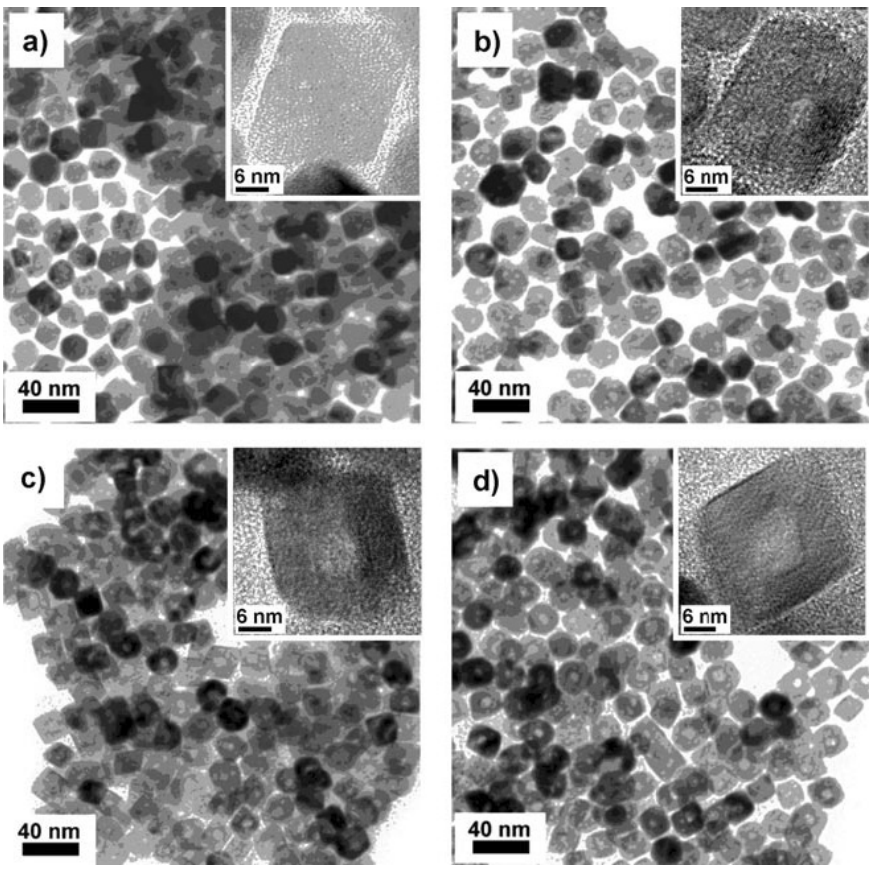

Figure 3.15. Evolution of fcc Co hollow nanoparallelepipeds with time. (a) TEM image of fcc CoO nanoparallelepipeds. (b), (c) TEM images of nanoparallelepipeds after heating fcc CoO at 290°C for (b) 1h and (c) 2h. (d) TEM image of fcc Co nanoparallelepipeds prepared after heating fcc CoO at 290°C for 2 h and then at 270°C for 1 h. A HRTEM image of each of the hollow nanoparallelepipeds is shown as an inset. [K.M. Nam, J.H. Shim, H. Ki, S. Choi, G. Lee, J. Jang, Y. Jo, M. Jung, H. Song, and J.T. Park, *Angew. Chem. Int.* Ed. **47**, 9504 (2008).]

followed by thermal treatment at 270°C for 1 h. The HRTEM image of each nanoparallelepiped is shown as an inset in Fig. 3.15. However, cobalt is not chemically or magnetically stable since it can be quickly oxidized.[38] Au, Pt, CdSe, and SiO_2 have been coated onto the Co nanoparticles to stabilize Co, however, this process results in polydispersed particles with nonuniform coatings and the magnetic moment is also reduced appreciably.[39–42]

Materials with high permeability value are very important for the development of portable communication. Homogeneous nanomaterials with a narrow distribution of local magnetic field are required to achieve the high permeability. FeCo alloy exhibits unique magnetic properties such as large permeability and high saturation magnetization which enables the FeCo alloy to generate strong magnetic field.[43] However, it is difficult to obtain monodisperse FeCo nanoparticles since FeCo can be easily oxidized. Several methods such as codecomposition of organometallic precursors under hydrogen[38] and chemical vapor deposition[44] have been utilized to complete this challenging task. FeCo combined with inert material including graphitic carbon, pyrolytic carbon or inert metals has attracted considerable interests.[38,45,46] FeCo/graphite nanocrystals have been fabricated via a scalable chemical vapour deposition method.[38] These nanocrystals with graphitic shell are soluble and stable in water, which makes them suitable for biological applications. Ultra-high magnetic saturation is achieved in these core–shell structured nanocrystals. These FeCo-based core–shell nanocrystals can be internalized in Mesenchymal stem cells, and magnetic-resonance images show enhanced negative-contrast. Such core–shell structures have been demonstrated to convert near-infrared (λ = 808 nm) optical energy to thermal energy, which can be used to release drug or destroy the cancer cells.[47–50]

In addition to FeCo alloy, core–shell structured Co-MFe_2O_4 (M = Fe, Mn) nanocomposites have been prepared through a seed mediate process introduced by Sun *et al*.[51,52] MFe_2O_4, or $MO{\cdot}Fe_2O_3$ has a cubic spinel structure. In this structure, oxygen ions form a close packing structure of FCC, and M^{2+} and Fe^{3+} ions occupy either tetrahedral or octahedral interstitial sites.[53,54] The size of the Co core ranges from 8 to 14 nm and the thickness of the shell ranges from 1 to 5 nm. This core–shell structure

exhibits an admirable magnetic property due to the Co core and shows improved chemical and magnetic stabilities due to the ferric shell.

Apart from cobalt, iron has a high magnetic moment density of 218 emu/g or 1713 emu/cc and is also magnetically soft as cobalt.[55] Iron nanoparticles dispersions with the size range below 20 nm are in the superparamagnetic regime and have high magnetic moment.[56] Iron nanoparticles can be synthesized via thermal decomposition of iron pentacarbonyl ($Fe(CO)_5$),[57–63] reductive decomposition of iron(II) bis(trimethylsilyl)amide ($Fe[NSi(CH_3)_3]_2]_2$),[64] and reduction of iron(III) acetylacetonate ($Fe(acac)_3$) or other iron salts.[65,66] However, the resulted iron nanoparticles are not stable as they can be easily oxidized. Thus Fe/Fe_3O_4 nanocomposites with core–shell structures have been synthesized by controlled oxidation, for more uniform dispersion and enhanced chemical stability. These core–shell nanoparticles enjoy multiple applications such as bioseparation, drug delivery, and biodetection when combined with biomolecules.

Snoeck *et al*. have utilized off-axis electron holography in a TEM to clarify the magnetic remnant configurations in single crystalline Fe nanocubes with a size of 30 nm. A ferromagnetic dipolar coupling is shown in two neighboring nanocubes with adjacent {100} surfaces. However, four cubes arranged in a square form exhibit a bending of the magnetic induction such as a magnetic flux closure state. Hollow Fe nanoframes have been fabricated by the decomposition of Fe (II)-stearate complex assisted with sodium oleate and oleic acid.[67] The formation of the nanoframes is ascribed to the presence of the sodium molten salt. This nanoframe can be used for drug delivery.

In addition to Fe nanomaterials, nanosized FePt is also studied. FePt nanocubes can be prepared at 205°C by controlling Fe/Pt ratio in the precursors and addition sequence of oleic acid and oleylamine.[68] An internal particle structure variation occurs in the FePt nanocubes after thermal annealing, which changes the nanocube assembly from superparamagnetic to ferromagnetic. Monodisperse and highly-crystalline $L1_0$-FePt nanocrystals have been synthesized via a SiO_2-nanoreactor strategy.[69] Even when the nanocrystals are heated at 900°C, there are no coalescence and coarsening due to the thick SiO_2 coating. The size of these nanocrystals is very small (6.5 nm), and the coercivity is very large (18.5 kOe)

which is attributed to the highly-crystalline nature. These monodisperse $L1_0$-FePt nanocrystals arrays can be used as recording media[70,71] with density beyond 1 Tb/ in.[71]

Other magnetic nanomaterials include SmCo-based nanomegnets that can be used in high-performance permanent magnets and high-density data storage media due to their large coercivity and high magnetic moment.[72–77] Hard magnetic nanocrystalline $SmCo_5$ (or Sm_2Co_{17}) particles have been prepared by high-temperature reductive annealing of the core/shell-structured Co/Sm_2O_3 nanoparticles.[78] The $SmCo_5$ exhibits a magnetic coercivity of 8 kOe at room temperature, which indicates the achievement of air-stable SmCo-based nanomegnets. More recently, air-stable SmCo nanoblade particles with high coercivity have been synthesized by a direct chemical method.[79] This method is benign to the environment and facile for large volume industrial synthesis.

3.2.4. *Synthesis of semiconductor nanoparticles*

In this section, the discussion will be focused on the synthesis of nonoxide semiconductor, whereas the formation of oxide semiconductor nanoparticles will be discussed in the following section, since the synthesis methods are significantly different from each other. Nonoxide semiconductor nanoparticles are commonly synthesized by pyrolysis of organometallic precursor(s) dissolved in anhydrate solvents at elevated temperatures in an airless environment in the presence of polymer stabilizer or capping material.[80–84] It should also be noted here that in the synthesis of metallic nanoparticles, polymer attached on the surface are commonly termed as polymer stabilizers. However, in the synthesis of semiconductor nanoparticles, polymers on the surface are generally referred to as capping materials. Capping materials are linked to the surface of nanocrystallites via either covalent bonds or other bonds such as dative bonds.[85] Examples are sulfur and transition metal ions and nitrogen lone pair of electrons form dative bond. The formation of monodispersed semiconductor nanocrystallites is generally achieved by the following approaches. First, temporally discrete nucleation is attained by a rapid increase in the reagent concentrations upon injection, resulting in an abrupt supersaturation. Second, Ostwald ripening during aging at

increased temperatures promotes the growth of large particles at the expense of small ones, narrowing the size distribution. Third, size selective precipitation is applied to further enhance the size uniformity. It is noted that although organic molecules are used to stabilize the colloidal dispersion, similar to that in the formation of metallic colloidal dispersions, the organic monolayers on the surfaces of semiconductor nanoparticles plays a relatively less significant role as a diffusion barrier during the subsequent growth of initial nuclei. This is simply because there is a less extent or negligible subsequent growth of initial nuclei due to the depletion of growth species and the drop of temperature at the nucleation stage.

Synthesis of CdE (E = S, Se, Te) semiconductor nanocrystallites reported by Murray *et al*.,[86] which is based on the earlier work by Steigerwald *et al*.[87,88] is used as an example to illustrate the general approach. Dimethylcadmium (Me_2Cd) was used as the Cd source and bis(trimethylsilyl) sulfide ($(TMS)_2S$), trioctylphosphine selenide (TOPSe), and trioctylphosphine telluride (TOPTe) were used as S, Se, and Te precursors, respectively. Mixed tri-*n*-octylphosphine (TOP) and tri-*n*-octylphosphine oxide (TOPO) solutions were used as solvents and capping materials.

The procedure for the preparation of TOP/TOPO capped CdSe nanocrystallites is briefly outlined below.[86] Fifty grams of TOPO is dried and degassed in the reaction vessel by heating to ~200°C at ~1 torr for ~20 min, flushing periodically with argon. The temperature of the reaction flask is then stabilized at ~300°C under ~1 atm of argon. 1.00 mL of Me_2Cd is added to 25.0 mL of TOP in the dry box, and 10.0 mL of 1.0 M TOPSe stock solution is added to 15.0 mL of TOP. Two solutions are then combined and loaded into a syringe in the dry box. The heat is removed from the reaction vessel. The syringe containing the reagent mixture is quickly removed from the dry box and its content delivered to the vigorously stirring reaction flask in a single injection through a rubber septum. The rapid introduction of the reagent mixture produces a deep yellow/orange solution with an absorption feature at 440–460 nm. This is also accompanied by a sudden decrease in temperature to ~180°C. Heating is restored to the reaction flask and the temperature is gradually raised to and aged at 230–260°C. Depending on the aging time, CdSe

nanoparticles with a series of sizes ranging from ~1.5 nm to 11.5 nm in diameter are prepared.

The above prepared colloidal dispersion is purified by cooling to ~60°C, slightly above the melting point of TOPO, and adding 20 mL of anhydrous methanol, which results in the reversible flocculation of the nanocrystallites. The flocculate is separated from the supernatant by centrifugation. Dispersion of the flocculation in 25 mL of anhydrous 1-butanol followed by further centrifugation results in an optically clear solution (more precisely speaking, a colloidal dispersion, but solution is a widely accepted term in the literature in this field) of nanocrystallites and a gray precipitate containing byproducts, consisting mostly of elemental Cd and Se, of the reaction. Addition of 25 mL of anhydrous methanol to the supernatant produces flocculation of the crystallites and removes excess TOP and TOPO. A final rinse of the flocculate with 50 mL of methanol and subsequent vacuum drying produces ~300 mg of free flowing TOP/TOPO capped CdSe nanocrystallite.

The purified nanocrystallites are subsequently dispersed in anhydrous 1-butanol forming an optically clear solution. Anhydrous methanol is then added drop wise to the dispersion until opalescence persists upon stirring or sonication. Separation of supernatant and flocculate by centrifugation produces a precipitate enriched with the largest crystallites in the sample. Dispersion of the precipitate in 1-butanol and size-selective precipitation with methanol is repeated until no further narrowing the size distribution as indicated by sharpening of optical absorption spectrum.

Mixed phosphine and phosphine oxide solutions were found to be good solvents for the high temperature growth and annealing of CdSe crystallite.[89,90] The coordinating solvent plays a crucial role in controlling the growth process, stabilizing the resulting colloidal dispersion, and electronically passivating the semiconductor surface.

Injection of reagents into the hot reaction vessel results in a short burst of homogeneous nucleation due to an abrupt supersaturation and simultaneously a sharp drop in temperature associated with the introduction of room temperature precursor solution. The depletion of reagents through such nucleation prevents further nucleation and also largely hinders the subsequent growth of existing nuclei. Monodispersion is further achieved by gently reheating the solution to promote slow growth of

initial nuclei. An increased temperature results in an increased solubility, and thus a reduced supersaturation of growth species in the solution. As a result, nuclei with small sizes may become unstable and dissolve back into the solution; dissolved species will then deposit onto the surfaces of large particles. This dissolution-growth process is also known as Ostwald ripening, in which large particles grow at the expanse of small particles.[91] Such a growth process would result in the production of highly monodispersed colloidal dispersions from systems that may initially be polydispersed.[92] Lowering the synthesis temperature results in a wider size distribution with an increased amount of small particles. A lowered temperature would result in an increased supersaturation favoring continued nucleation with smaller sizes. An increased temperature will promote the growth of nanoparticles with a narrow size distribution.

Size-selective precipitation would further narrow the size distribution of the colloids prepared. For the fractionation process to work well it is crucially important that the shape and surface derivation of the initial crystallites be uniform and that the initial polydispersity in size be relatively small.[86] It should be noted that although the subsequent growth of initial nuclei appears less important in the synthesis of monodispersed CdSe nanocrystallites as compared to that in the formation of monodispersed metal nanoparticles, due to the depletion of reagents as discussed above, the capping material provides an important steric barrier for diffusion and thus favored the diffusion-controlled subsequent growth of existing nuclei.

Size-selectively reprecipitation is a very useful method in the synthesis of monodispersed nanocrystals. For example, Guzelian *et al*.[93] prepared monodispersed InP nanocrystals of 2 to 5 nm in diameter via the reaction of $InCl_3$ and $P(Si(CH_3)_3)_3$ in trioctylphosphine oxide (TOPO) at elevated temperatures, and monodispersion is largely achieved by repeated size-selective reprecipitation. Since the synthesis is a slow process in which nucleation and growth occur simultaneously over long time scales, in contrast to temporally discrete nucleation and negligible subsequent growth in the synthesis of CdSe described above, InP nanoparticles have a broad size distribution. InP nanocrystals capped with dodecylamine are soluble in toluene and insoluble in methanol. Using stepwise addition of methanol to the reaction solution results in the

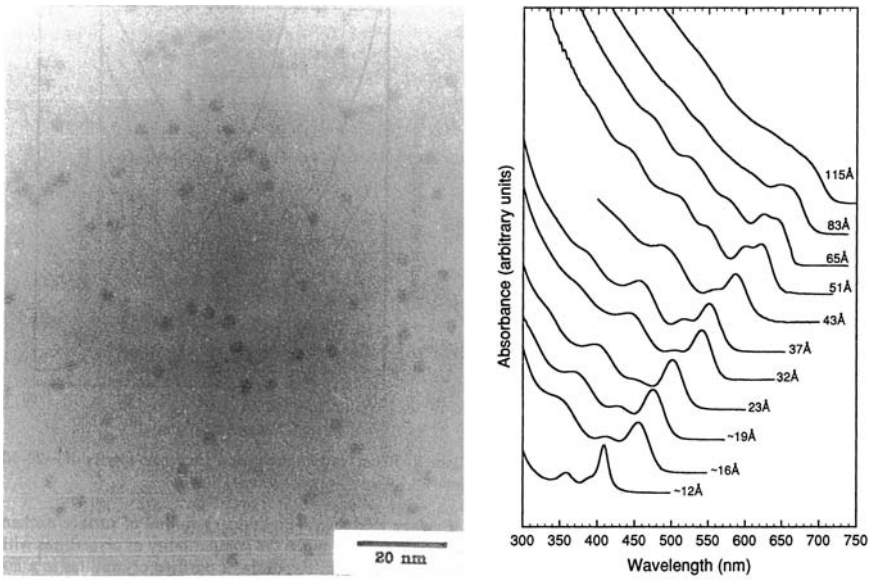

Figure 3.16. (a) A near monolayer of 51 Å diameter CdSe crystallites showing short-range hexagonal close packing. (b) Room temperature optical absorption spectra of CdSe nanocrystallites dispersed in hexane and ranging in size from ~12 to 115 Å. [C.B. Murray, D.J. Norris, and M.G. Bawendi, *J. Am. Chem. Soc.* **115**, 8706 (1993).]

incremental size-selective precipitation of the nanocrystals. From the same reaction mixture, isolated 2–5 nm nanocrystals are obtained, and if small enough volumes of methanol are used, a sufficiently careful precipitation series can resolve size distributions separated by as little as 0.15 nm.[93] Figure 3.16 shows the SEM images and optical absorption spectra of CdSe nanocrystallites in size ranging from ~1.2 nm to 11.5 nm and dispersed in hexane.[86]

Figure 3.17 shows the X-ray powder diffraction spectra of CdSe crystallites ranging from ~1.2 to 11.5 nm in diameter, and indicates CdSe crystallites have a predominantly wurtzite crystal structure with the lattice spacing of the bulk material.[86] Finite size broadening in all diffraction peaks are evident, and excessive attenuation and broadening in (102) and (103) peaks are characteristic of stacking faults along the (002) axis.[94]

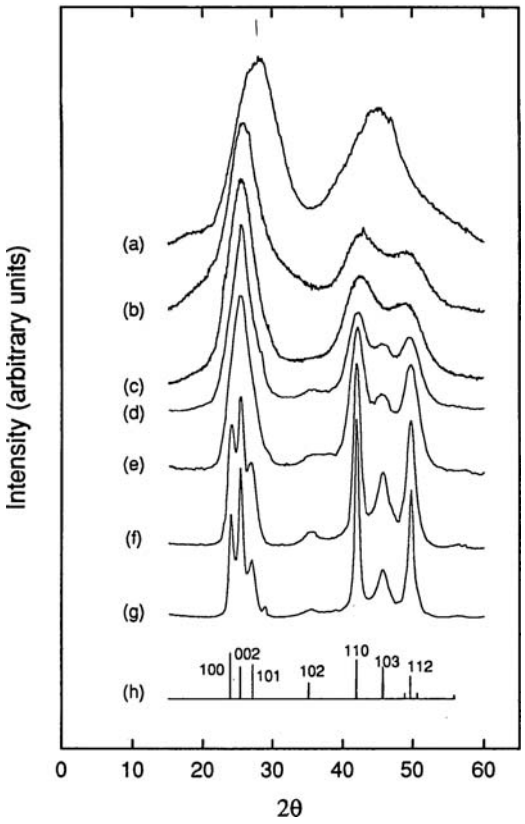

Figure 3.17. Powder X-ray diffraction spectra of (a) 12, (b) 18, (c) 20, (d) 37, (e) 42, (f) 83, and (g) 115 Å diameter CdSe nanocrystallintes compared with the bulk wurtzite peak positions (h). [C.B. Murray, D.J. Norris, and M.G. Bawendi, *J. Am. Chem. Soc.* **115**, 8706 (1993).]

Such defects are observed in high-resolution TEM image as shown in Fig. 3.18.[86]

Thermal decomposition of complex precursor in a high-boiling solvent represents another method in the production of compound semiconductor nanoparticles with a narrow size distribution.[95,96] For example, when $GaCl_3$ is mixed with $P(SiMe_3)_3$ in a molar ratio of Ga:P of 1:1 in toluene at room temperature, a complex Ga and P precursor, $[Cl_2GaP(SiMe_3)_2]_2$ forms.[97,98] Similar reactions may occur by mixing

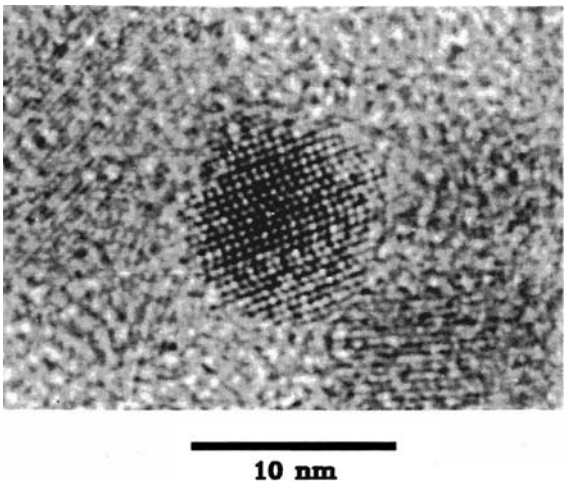

Figure 3.18. An 80 Å diameter CdSe crystallite imaged in bright field with atom contrast shows the presence of stacking faults in the (002) direction. [C.B. Murray, D.J. Norris, and M.G. Bawendi, *J. Am. Chem. Soc.* **115**, 8706 (1993).]

chloroindium oxalate and $P(SiMe_3)_3$ in a predetermined molar ratio in CH_3CN for the formation of InP complex precursor, or mixing chlorogallium oxalate, chloroindium oxalate, and $P(SiMe_3)_3$ in a desired molar ratio in toluene at room temperature.[95] The formation of InP, GaP and $GaInP_2$ high-quality nanocrystallites by heating the complex precursor dissolved in high-boiling solvent containing a mixture of TOP and TOPO as a colloidal stabilizer at elevated temperatures for several days. The typical thermal decomposition of InP precursor solution in TOP/TOPO at elevated temperatures produces InP nanocrystals capped with TOPO[96]:

$$\text{InPprecursor} + (C_8H_{17})_3PO \rightarrow \text{InP}–(C_8H_{17})_3PO + \text{byproducts}. \quad (3.37)$$

Such prepared nanoparticles of InP, GaP and $GaInP_2$ are well-crystallized with bulk zinc blende structure. Increase in heating duration was found to improve the crystallinity of the nanoparticles. Different particle sizes ranging from 2.0 to 6.5 nm are obtained by changing the precursor concentration or by changing the temperature. The narrow size distribution is achieved due to (1) the slow process rate of the decomposition reaction of

the complex precursors and possibly (2) the steric diffusion barrier of the TOP and TOPO stabilizer monolayer on the growing surface of nanoparticles.[95] The addition of methanol into the colloidal solution results in the precipitation of nanoparticles.

Thermal decomposition of complex precursors is also applied in the synthesis of GaAs nanoparticles.[99,100] For example, when an appropriate amount of $Li(THF)_2As(SiMe_3)_2$ (THF = tetrahydrofuran and Me = methyl) is added to a pentane solution of $[C_5Me_5)_2GaCl]_2$, followed by filtration, evaporation of the solvent, and recrystallization, pure arsinogallane complex precursor, $(C_5Me_5)Ga\text{-}As(SiMe_3)_2$ is produced. This complex precursor, when dissolved in organic solvents such as alcohol, undergoes thermal decomposition to form GaAs nanoparticles when heated above 60°C or exposed to air.[99] When tris(trimethylsilyl)arsine reacts with gallium chloride, complex GaAs precursors can be prepared.[101] GaAs nanocrystals can be prepared by heating the above complex precursor dissolved in polar organic solvents, such as in quinoline at 240°C for three days.[100]

Colloidal CdS and PbS dispersions with particle sizes ≤ 8 nm were prepared by mixing $Cd(OOCCH_3)_2.2H_2O$ or $Pb(OOCCH_3)_2.3H_2O$ with surfactants and thioacetamide (CH_3CSNH_2) in methanol solution.[102] Surfactants used in the preparation of CdS and PbS nanoparticles include: acetylacetone, 3-aminopropyltriethoxysilane, 3-aminopropyltrimethoxysilane, and 3-mercaptopropyltrimethoxysilane (MPTMS). Among these surfactants, MPTMS was found to be the most effective surfactant in the preparation of nanoparticles of CdS and PbS, which agreed with other group.[103]

CdS nanoparticles can be synthesized by mixing of $Cd(ClO_4)_2$ and $(NaPO_3)_6$ solutions with pH adjusted with NaOH and bubbled with argon gas. Desired amount of H_2S was injected into the gas phase and the solution was vigorously shaken.[89] The starting pH value was found to have a significant influence on the average size of the particles synthesized. The particle size increases with a decreasing starting pH value, and Fig. 3.19 shows the absorption and fluorescence spectra of the three CdS colloidal dispersions with different starting pH values.[89] For the smallest particle, i.e., for sample, the onset of absorption is already shifted to a wavelength clearly shorter than 500 nm.

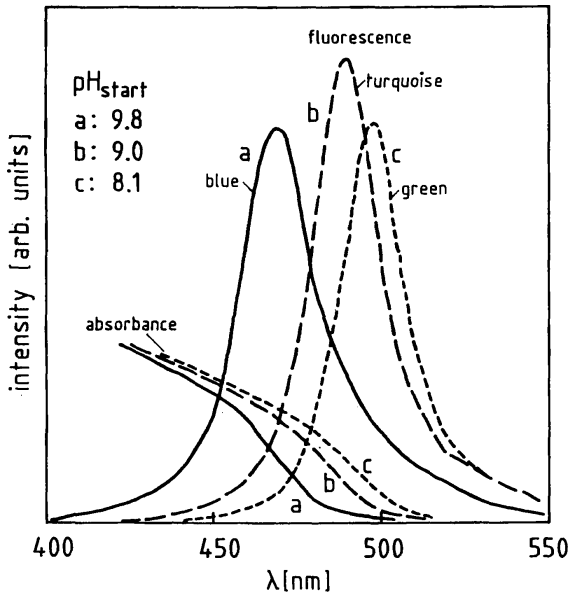

Figure 3.19. Absorption and fluorescence spectra of the three CdS colloidal dispersions with different starting pH values. The particle size increases with a decreasing starting pH value. [L. Spanhel, M. Haase, H. Weller, and A. Henglein, *J. Am. Chem. Soc.* **109**, 5649 (1987).]

Synthesis of GaN nanocrystallites poses a different challenge. Typically GaN would form at temperatures higher than 600°C.[104,105] Even thermal pyrolysis of complex precursors such as $[H_2GaNH_2]_3$ and $Ga(C_2H_5)_3NH_3$ which already have Ga–N bond requires a post heat treatment at temperatures above 500°C.[106,107] The reaction of Li_3N with $GaCl_3$ in benzene at 280°C under pressure in an autoclave produces nanocrystallite GaN through a liquid–solid reaction[108]:

$$GaCl_3 + Li_3N \rightarrow GaN + 3LiCl. \tag{3.38}$$

Such formed GaN nanocrystallites are of ~30 nm in diameter with mainly hexagonal structure with a small fraction of rock salt-phase with lattice constants close to that of bulk materials.[108]

Solution synthesis of colloidal GaN.[109,110] For example, Micic *et al.*[109] synthesized colloidal GaN nanoparticles of 3.0 nm in diameter with spherical

shape and zinc-blende crystal structure. First a GaN complex precursor, polymeric gallium imide, $\{Ga(NH)_{3/2}\}_n$, was prepared by the reaction of dimeric amidogallium, $Ga_2[N(CH_3)_2]_6$, with gaseous ammonia, NH_3, at room temperature.[111,112] The precursor was then heated in trioctylamine (TOA) at 360°C for 24 h to produce GaN nanocrystals under flowing ammonia at ambient pressure. The solution was cooled to 220°C and a mixture of TOA and hexadecylamine (HAD) was added and stirred at 220°C for 10 h. The GaN nanocrystals were capped with a mixture of TOA and HAD.

3.2.5. *Synthesis of oxide nanoparticles*

Compared to the synthesis of metallic and nonoxide nanoparticles, the approaches used in the fabrication of oxide nanoparticles are less elaborated and there are less defined general strategies for the achievement of monosized distribution. Although all the fundamental considerations, including a burst of homogeneous nucleation and diffusion-controlled subsequent growth, are applicable to the oxide systems, the practical approaches vary noticeably from system to system. Reaction and growth in the formation of oxide nanoparticles are more difficult to manipulate, since oxides are generally more stable thermally and chemically than most semiconductors and metals. For example, Ostwald ripening is applied in the synthesis of oxide nanoparticles to reduce size distribution; the results may be less effective as in other materials. The most studied and best-established example of oxide colloidal is silica colloids[113] and various oxide nanoparticles have been studied.[114,115] Commonly oxide particles in colloidal dispersions are synthesized by sol–gel processing. Sol–gel processing is also commonly used in the fabrication of various core–shell nanostructures[116] and surface engineering of nanostructures.[117] Before discussing the general approaches for the synthesis of oxide nanoparticles, let us briefly discuss the sol–gel process first.

3.2.5.1. *Introduction to sol–gel processing*

Sol–gel processing is a wet chemical route for the synthesis of colloidal dispersions of inorganic and organic-inorganic hybrid materials,

particularly oxides and oxide-based hybrids. From such colloidal dispersions, powders, fibers, thin films, and monoliths can be readily prepared. Although the fabrication of different forms of final products requires some specific considerations, fundamentals and general approaches in the synthesis of colloidal dispersions are the same. Sol–gel processing offers many advantages, including low processing temperature and molecular level homogeneity. Sol–gel processing is particularly useful in making complex metal oxides, temperature sensitive organic-inorganic hybrid materials, and thermodynamically unfavorable or metastable materials. For more details, readers may wish to consult the abundant literature in this field. For instance, *Sol–Gel Science* by Brinker and Scherer,[118] Introduction to *Sol–Gel Processing* by Pierre,[119] and *Sol–Gel Materials* by Wright and Sommerdijk[120] provide an excellent and comprehensive coverage on sol–gel processing and materials. Typical sol–gel processing consists of hydrolysis and condensation of precursors. Precursors can be either metal alkoxides or inorganic and organic salts. Organic or aqueous solvents may used to dissolve precursors, and catalysts are often added to promote hydrolysis and condensation reactions:

Hydrolysis:

$$M(OEt)_4 + x\,H_2O \rightarrow M(OEt)_{4-x}(OH)_x + x\,EtOH. \tag{3.39}$$

Condensation:

$$M(OEt)_{4-x}(OH)_x + M(OEt)_{4-x}(OH)_x \rightarrow (OEt)_{4-x}(OH)_{x-1}\,M - O - M(OEt)_{4-x}(OH)_{x-1} + H_2O. \tag{3.40}$$

Hydrolysis and condensation reactions are both multiple-step processes, occurring sequentially and in parallel. Each sequential reaction may be reversible. Condensation results in the formation of nanoscale clusters of metal oxides or hydroxides, often with organic groups embedded or attached to them. These organic groups may be due to incomplete hydrolysis, or introduced as nonhydrolysable organic ligands. The size of the nanoscale clusters, along with the morphology and microstructure of the final product, can be tailored by controlling the hydrolysis and condensation reactions.

For the synthesis of colloidal dispersions of multiple component materials, the challenges are to ensure heterocondensation reactions between different constituent precursors, which typically have different chemical reactivity. The reactivity of a metal atom is dependent largely on the extent of charge transfer and the ability to increase its coordination number. As a rule of thumb, the electronegativity of a metal atom decreases and the ability to increase its coordination number increases with their ionic radius as shown in Table 3.3.[121] Accordingly the chemical reactivity of the corresponding alkoxides increases with their ionic radius. There are several ways to ensure heterocondensation, and achieve a homogeneous mixture of multiple components at the molecular/atomic level.

First, the precursors can be modified by attaching different organic ligands. For a given metal atom or ion, large organic ligand or more complex organic ligand would result in a less reactive precursor.[118] For example, $Si(OC_2H_5)_4$ is less reactive than $Si(OCH_3)_4$, and $Ti(OPr^x)_4$ is less reactive than $Ti(OPr^i)_4$. Another way to control the reactivity of the alkoxides is to chemically modify the coordination state of the alkoxides with a chelating agent such as acetylacetone. Multiple step sol–gel processing is yet another way to overcome this problem. The less reactive precursor is first partially hydrolyzed, and more reactive precursor is hydrolyzed later.[122] In more extreme cases, one precursor can be fully hydrolyzed first and all water is depleted, if hydrolyzed precursor has a very low condensation rate, then the second precursor is introduced and forced to condensate with the hydrolyzed precursor by the reaction:

$$M(OEt)_4 + xH_2O \rightarrow M(OH)_4 + 4HOEt. \tag{3.41}$$

Table 3.3. Electronegativity, χ, partial charge, δM, ionic radius, r, and coordination number, n, of some tetravalent metals.[121]

Alkoxide	χ	δM	r(Å)	n
$Si(OPr^i)_4$	1.74	+0.32	0.40	4
$Ti(OPr^i)_4$	1.32	+0.60	0.64	6
$Zr(OPr^i)_4$	1.29	+0.64	0.87	7
$Ce(OPr^i)_4$	1.17	+0.75	1.02	8

where OPr^i is $OCH_2CH_2CH_3$.

Condensation reactions are only limited between hydrolyzed less reactive precursor with more reactive precursor:

$$M(OH)_4 + M'(OEt)_4 \rightarrow (HO)_3\text{–}M\text{–}O\text{–}M'\text{–}(OEt)_3. \quad (3.42)$$

Incorporating organic components into an oxide system by sol–gel processing makes it easy to form organic-inorganic hybrids. One approach is to copolymerize or cocondense both the inorganic precursor(s), which lead to the formation of the inorganic component, and the organic precursor(s), which consist of nonhydrolysable organic groups. Such organic-inorganic hybrids are a single-phase material, in which the organic and inorganic components are linked through chemical bonds. Another approach is to trap the desired organic components physically inside the inorganic or oxide network, by either homogeneously dispersing the organic components in the sol, or infiltrating the organic molecules into the gel network. Similar approaches can be applied for the incorporation of biocomponents into oxide systems. Another method to incorporate biocomponents into the oxide structure is to use functional organic groups to bridge inorganic and biological species. Organic-inorganic hybrid materials form a new family of materials, which promise a lot of important potential applications and will be discussed further in Chapter 6.

Another challenge in making complex oxide sols is that the constituent precursors may exert a catalytic effect on one another. As a result, the hydrolysis and condensation reaction rates when two precursors are mixed together may be significantly different from those when the precursors are processed separately.[123] In the sol preparation, not much attention has been paid to the control of crystallization or formation of crystal structure, although the formation of crystalline structure of complex oxides without high-temperature firing is desired for some applications. Matsuda and coworkers have demonstrated that it is possible to form the crystalline phase of $BaTiO_3$ without high temperature sintering by carefully controlling processing conditions, including concentrations and temperature.[124] However, there is still a lack of general understanding on the control of crystallization of complex oxides during sol preparation.

By a careful control of sol preparation and processing, monodispersed nanoparticles of various oxides, including complex oxides, organic-inorganic hybrids, and biomaterials, can be synthesized. The key issue is to promote temporal nucleation followed with diffusion-controlled subsequent growth.[125–127] The particle size can be varied by changing the concentration and aging time.[118] In a typical sol, nanoclusters formed by hydrolysis and condensation reactions commonly have a size ranging from 1 to 100 nm.

It should also be noted that in the formation of monodispersed oxide nanoparticles, the stabilization of colloids is generally achieved by electrostatic double layer mechanism. Therefore, the polymer steric diffusion barrier that existed in the formation of metal and nonoxide semiconductor colloids, is generally not present in the formation of metal oxides. So the diffusion-controlled growth is achieved through other mechanisms, such as controlled release and a low concentration of growth species in the sol.

3.2.5.2. *Forced hydrolysis*

The simplest method for the generation of uniformly sized colloidal metal oxides is based on forced hydrolysis of metal salt solutions. It is well-known that most polyvalent cations readily hydrolyze, and that deprotonation of coordinated water molecules is greatly accelerated with increasing temperature. Since hydrolysis products are intermediates to precipitation of metal oxides, increasing temperature results in an increasing amount of deprotonated molecules. When the concentration far exceeds the solubility, nucleation of metal oxides occurs. In principle, to produce such metal oxide colloids, one just need to age hydrolyzed metal solutions at elevated temperatures. It becomes obvious that hydrolysis reaction should proceed rapidly and produce an abrupt supersaturation to ensure a burst of nucleation, resulting in the formation of a large number of small nuclei and eventually leading to the formation of small particles. This principle was demonstrated in the pioneer work on the formation of silica spheres by Stöber and coworkers.[127]

The procedures for the preparation of silica spheres were simple and straightforward. Various silicon alkoxides with different alkyl ligand sizes

were used as precursors, ammonia was used as a catalyst, and various alcohols were used as solvents. First alcohol solvent, ammonia, and a desired amount of water were mixed, and then silicon alkoxide precursor was added under vigorous stirring. The formation of colloids or the change of solution optical appearance became noticeable just in a few minutes after the addition of precursors. Depending on the precursors, solvents, and the amounts of water and ammonia used, spherical silica particles with mean sizes ranging from 50 nm to 2 μm were obtained. Figure 3.20 shows the first example of such prepared silica spheres.[127]

It was found that the reaction rate and particle size were strongly dependent on solvents, precursors, amount of water, and ammonia. For the different alcoholic solvents, reaction rates were fastest with methanol, slowest with *n*-butanol. Likewise, final particle sizes obtained under comparable conditions were smallest in methanol and biggest in *n*-butanol. However, there was a tendency toward wide size distributions with the higher alcohols. Similar relationship with regard to reaction rates and particle sizes was found when comparing results with different ligand sizes in the precursors. Smaller ligand resulted in faster reaction rate and

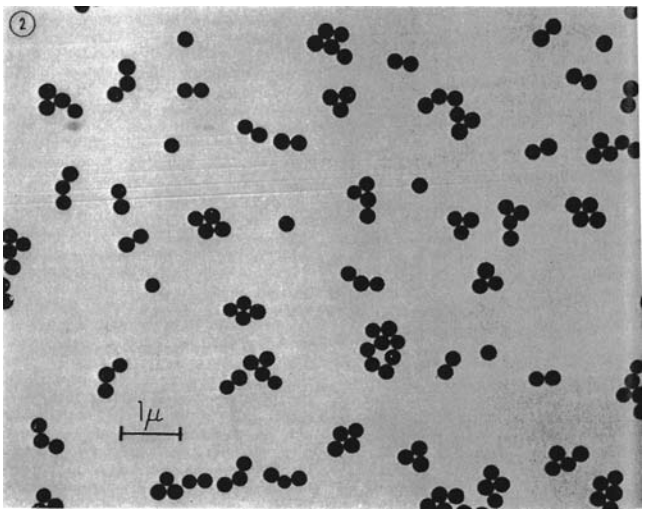

Figure 3.20. SEM micrograph of silica spheres prepared in the ethanol-ethyl ester system. [W. Stober, A. Fink, and E. Bohn, *J. Colloid Interf. Sci.* **26**, 62 (1968).]

smaller particle size, whereas larger ligands led to slower reaction rate and large particle size. Ammonia was found to be necessary for the formation of spherical silica particles, since condensation reaction under a basic condition yields three-dimensional structure instead of a linear polymeric chain which occurs under an acidic condition.[118]

Both hydrolysis and condensation reactions, as any other chemical reactions, are strongly dependent on reaction temperatures. An elevated temperature would result in a drastic increase of reaction rate. Preparation of spherical colloidal α-Fe_2O_3 nanoparticles of 100 nm in size can be used as another example to illustrate the typical procedure of forced hydrolysis.[128] First $FeCl_3$ solution is mixed with HCl, and diluted. The mixture is then added into preheated H_2O at 95–99°C with constant stirring. The solution is kept in a sealed preheated bottle at 100°C for 24 h before quenched in cold water. The high temperature favors a fast hydrolysis reaction and results in the high supersaturation, which in turn leads to the formation of a large number of small nuclei. Dilution before heating to high temperatures is very important to ensure a controlled nucleation and subsequent diffusion-limited growth. A long aging period would permit the occurrence of Ostwald ripening to further narrow the size distribution.

The nanoparticles of iron oxide and their aqueous dispersions have attracted tremendous interests for their potential use in magnetic nanodevice and biomagnetic applications.[129] In the study of Sun *et al*., various monodispersed MFe_2O_4 (M = Fe, Co, Mn) particles have been prepared via an organic phase process through the reaction of metal acetylacetonate and 1,2-hexadecanediol. The size of the particles can be controlled in the range of 3 to 20 nm. Furthermore, these nanoparticles can turn from hydrophobic to hydrophilic by mixing with tetramethylammonium 11-aminoundecanoate, which is a bipolar surfactant. These aqueous nanoparticles can be uitilized in magnetic and biomagnetic nanodevice. The shape-controlling preparation of $MnFe_2O_4$ has also been studied by varying the concentrations of the reactants in a one-pot reaction.[130]

3.2.5.3. *Controlled release of ions*

Controlled release of constituent anions and/or cations has a significant influence on the kinetics of nucleation and subsequent growth of oxide

nanoparticles, and is achieved by the spontaneous release of anions from organic molecules. For example, it is well-known that solutions of urea, $CO(NH_2)_2$, when heated liberate hydroxide ions, which can cause precipitation of metal oxide or hydroxide.[131–133] For example, the decomposition of urea is used to control the nucleation process in the synthesis of Y_2O_3:Eu nanoparticles.[132] Yttrium and europium chlorides were dissolved in water and the pH was adjusted to ~1 with hydrochloride acid or potassium hydroxide. An excess of urea, typically 15x, was dissolved into the solution. The solution was then raised to > 80°C for 2 h. The urea decomposed slowly and there was a burst of nucleation when a certain pH value of ~4–5 was reached.

In general, a certain types of anions are commonly introduced into the system as a catalyst. In addition to the catalytic effect, anions commonly exert other influences on the processing and the morphology of the nanoparticles.[134] Figure 3.21 shows the TEM images of particles obtained from solutions of $FeCl_3$ and HCl under various conditions listed in Table 3.4.[134,135] Systems a, b, and c represent hematite (α-Fe_2O_3) dispersions, where system d is rod-like akageneite, β-FeO(OH). Presence of anions may result in a change of the surface properties and interface energy of nanoparticles, and subsequently influence the growth behavior of the particle. Anions may be incorporated into the structure of nanoparticles, or adsorbed onto the surface of nanoparticles. Anions may also have significant influences on the stability of the colloidal dispersion, when nanoparticles are stabilized by electrostatic stabilization mechanism.

The preparation of crystalline ZnO nanoparticles is another example of controlled release of anions. First zinc acetate is dissolved into methanol to form zinc alkoxide precursor solution and then zinc alkoxide precursor is hydrolyzed and condensed to form zinc oxide colloid with lithium hydroxide as a catalyst with sonication at 0°C or room temperature.[136,137] Sonication accelerates the release of OH^- groups, resulting in immediate reaction to form a stable ZnO sol. Use of NaOH, KOH, or $Mg(OH)_2$ all produces turbid precipitates. ZnO nanoparticles are ~3.5 nm in diameter in fresh sols and ~5.5 nm in 5 day old ones. Aging of alcoholic ZnO colloids is known to produce larger particles.[138–140] Acetate groups are believed to attach to the surface of ZnO colloids and thus stabilize the colloidal dispersion.[136,140]

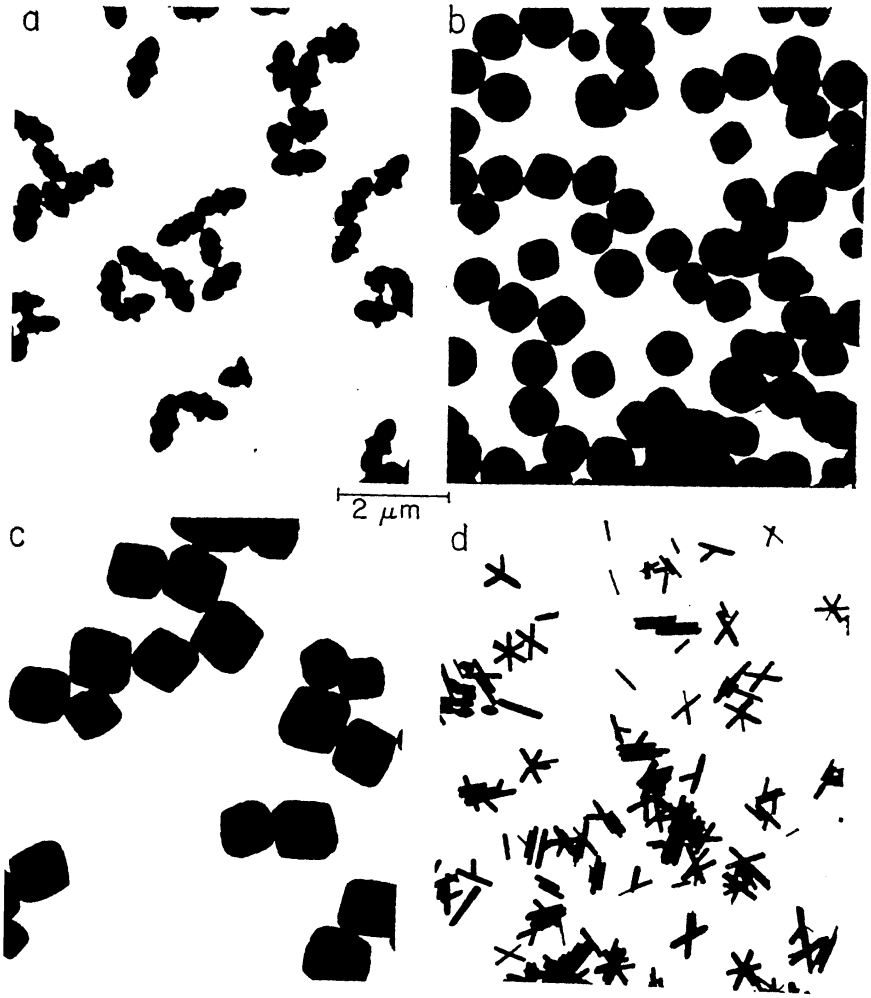

Figure 3.21. TEM images of various iron oxide and iron hydroxide nanoparticles obtained from solutions of $FeCl_3$ and HCl under various conditions listed in Table 3.4. [E. Matijević, *J. Colloid Interf. Sci.* **58**, 374 (1977).]

3.2.6. *Vapor phase reactions*

Nanoparticles can also be synthesized by vapor phase reactions, following the same mechanisms discussed in the synthesis of nanoparticles in liquid medium. In general, reaction and synthesis are carried out at elevated

Table 3.4. A summary of synthesis parameters including temperature and time of aging used to obtain α-Fe_2O_3 (A, B, and C) or β-FeO(OH) nanoparticles shown in Fig. 3.19.[134,135]

	Fe^{3+} (M)	Cl^- (M)	Initial pH	Final pH	Temp (°C)	Time
A	0.018	0.104	1.3	1.1	100	24 h
B	0.315	0.995	2.0	1.0	100	9 days
C	0.09	0.28	1.65	0.88	100	24 h
D	0.09	0.28	1.65	0.70	100	6 h

temperatures and under a vacuum. Vacuum is needed to ensure a low concentration of growth species so as to promote diffusion-controlled subsequent growth. Grown nanoparticles are normally collected on a non-sticking substrate placed down stream at a relatively low temperature. Obviously only do a small fraction of nanoparticles settle on the substrate surface. Furthermore, the nanoparticles settled on the substrate surface may not represent the true particle size distribution. It is also difficult to introduce stabilization mechanism during synthesis to prevent the formation of agglomerates. Despite of the aforementioned challenges, it has been demonstrated that various nanoparticles can be synthesized by vapor phase reactions. For example, the gas aggregation technique has been applied in the synthesis of silver nanoparticles of 2~3 nm in diameter.[141] Another example is the production of highly dispersed silica particles less than 100 nm in diameter by combustion of silicon tetrachloride in a hydrogen torch.[142]

It is noted that nanoparticles, formed through homogeneous nucleation and then deposited on substrates, may migrate and agglomerate.[143] Two types of agglomerates were found. One is the large size spherical particle and another is the needle-like particle. The formation of prolate particles commonly along step edges were found in the systems of Au on (100) NaCl[144] and (111) CaF[145] substrates, and Ag on (100) NaCl substrates.[141] However, the step edges are not always required for the formation of needle-like crystals. For example, crystal CdS nanorods with a length up to several hundred micrometers were formed.[146] Au particles with diameters in a few nanometers have been grown on various oxide substrates including iron oxide,[147] γ-alumina,[148] and titania.[149]

GaAs nanoparticles can be synthesized by homogeneous vapor phase nucleation from organometallic precursors.[150] Trimethyl gallium and AsH_3

are used as precursors and hydrogen is used as a carrier gas as well as a reduction reagent. Reaction and nucleation occur at a temperature of 700°C at atmospheric pressure. GaAs nanoparticles are collected thermophoretically on a holey carbon film downstream at a temperature of 350°C. The nanoparticles is found to compose of highly faceted single crystal GaAs with diameters ranging from 10 to 20 nm. In addition, an increase in reaction and nucleation temperature results in an increased particle size. An increased concentration of precursors has the similar influence on the particle size. However, change in temperature and precursor concentrations is found to have negligible influence on the morphology of nanoparticles.

3.2.7. *Solid-state phase segregation*

Quantum dots of metals and semiconductors in glass matrix are commonly formed by homogeneous nucleation in solid-state.[151,152] First the desired metal or semiconductor precursors were introduced to and homogeneously distributed in the liquid glass melt at high temperatures during glass making, before quenching to room temperature. Then the glass was annealed by heating to a temperature about the glass transition point and held for a predesigned period of time. During the annealing, metal or semiconductor precursors were converted to metals and semiconductors. As a result, supersaturated metal or semiconductors formed nanoparticles through nucleation and subsequent growth via solid-state diffusion.

Homogeneous glasses are made by dissolving metals, in the form of ions, in the glass melts and then rapidly cooled to room temperature. In such glasses metals remain as ions.[153] Upon reheating to an intermediate temperature region, metallic ions are reduced to metallic atoms by certain reduction agents such as antimony oxide that is also added into the glasses. Metallic nanoparticles can also be nucleated by ultraviolet, X-ray, or γ-ray radiation if a radiation-sensitive ion such as cerium is present.[153] The subsequent growth of the nuclei takes place by solid-state diffusion.[154] For example, glasses with nanoparticles of gold,[153] silver,[155] and copper[156] can all be prepared in such an approach. Although metallic ions may be highly soluble in the glass melts or glasses, metallic atoms are not soluble in glasses. When heated to elevated temperatures, metallic atoms acquire needed diffusivity to migrate through the glasses and

subsequently form nuclei. These nuclei would grow further to form nanoparticles of various sizes. Since solid-state diffusion is relatively slow, it is relatively easy to have a diffusion-controlled growth for the formation of monosized particles. Figure 3.22 shows the SEM micrograph of Cu and Ag nanoparticles in glass matrices.[157]

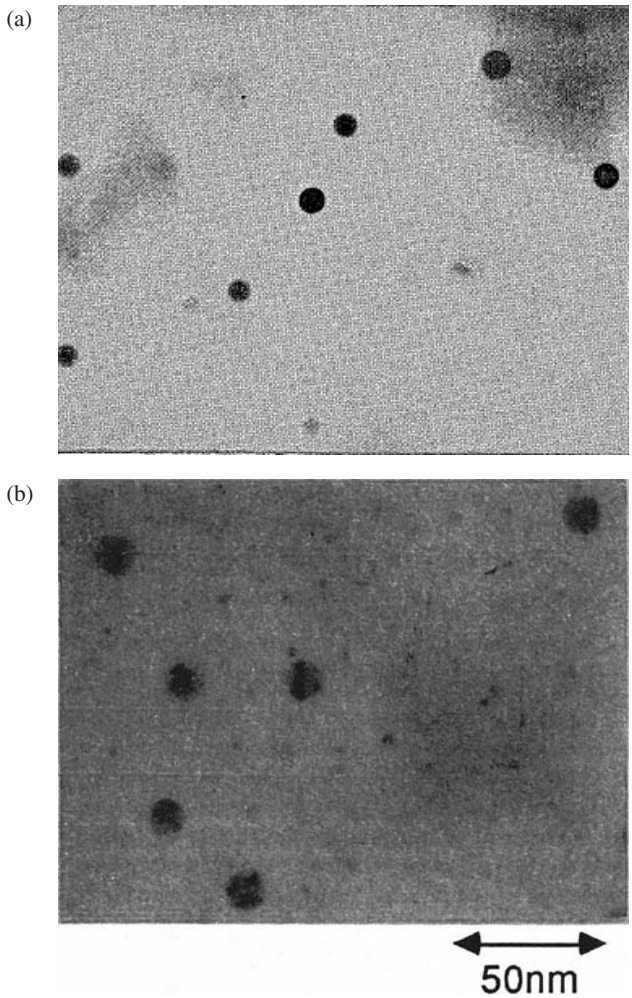

Figure 3.22. TEM micrograph of Cu and Ag nanoparticles in $BaO\text{-}P_2O_5$ glass: (a) $50P_2O_5$-50BaO-6SnO-$6Cu_2O$ and (b) $50P_2O_5$-50BaO-4SnO-$4Ag_2O$. [K. Uchida, S. Kaneko, S. Omi, C. Hata, H. Tanji, Y. Asahara, and A.J. Ikushima, *J. Opt. Soc. Am.* **B11**, 1236 (1994).]

Nanoparticles dispersed in glass matrix can be synthesized through sol–gel processing as well. There are two approaches: (1) mixing pre-synthesized colloidal dispersion with matrix sol before gelation, and (2) making a homogeneous sol containing desired ions for the formation of nanoparticles first and annealing the solid product at elevated temperatures.

For example, silica glasses doped with $Cd_xZn_{1-x}S$ were prepared by hydrolysis and polymerization of tetraethoxylsilane, $Si(OC_2H_5)_4$, TEOS, cadmium acetate, $Cd(CH_3COO)_2{\cdot}2H_2O$, zinc acetate, $Zn(CH_3COO)_2{\cdot}2H_2O$ in dimethylsufphoxide (DMSO), which serves as both solvent and sulfur precursor.[158] First cadmium and zinc precursors were dissolved into DMSO. When a homogenous solution was attained, TEOS and water was then added. The mixture was refluxed at 80°C for two days. The dry gels were first heat treated at 350°C in air to eliminate the residual organics and then heated again at 500 and 700°C in nitrogen for 30 min at each temperature. The gels before firing at elevated temperatures were colorless and transparent, indicating a homogeneous glass phase with absence of $Cd_xZn_{1-x}S$ nanoparticles. Glasses become yellow, when fired at 500°C in nitrogen, indicating the formation of $Cd_xZn_{1-x}S$ nanoparticles.

Nanoparticles of metals in polymer matrix can be synthesized through the reduction of metal ions by growing polymer chain radicals.[159–162] Typical preparative procedure can be illustrated by taking the synthesis of Ag nanoparticles in poly(methylmethacrylate) (PMMA) as an example. Silver trifluoroacetate ($AgCF_3CO_2$, AgTfa) and radical polymerization initiators, either $2,2'$-azobisisobuyronitrile (AIBN) or benzoyl peroxide (BPO), were dissolved into methylmethacrylate (MMA). The solution was then heated at 60°C for over 20 h to complete the polymerization of MMA; the resulting Ag-PMMA samples were further heat-treated at 120°C (which is slightly above the glass transition temperature of PMMA) for another 20 h. In such a process, the metal ions were reduced to metal atoms by the growing polymer chain radicals, and consequently metal atoms nucleated to form nanoparticles. The post heating at higher temperatures was considered to promote further growth of already formed metallic nuclei. However, it is not clear how much is the enlargement of the nanoparticle size and the evolution of particle size distribution during such a post heat-treatment.

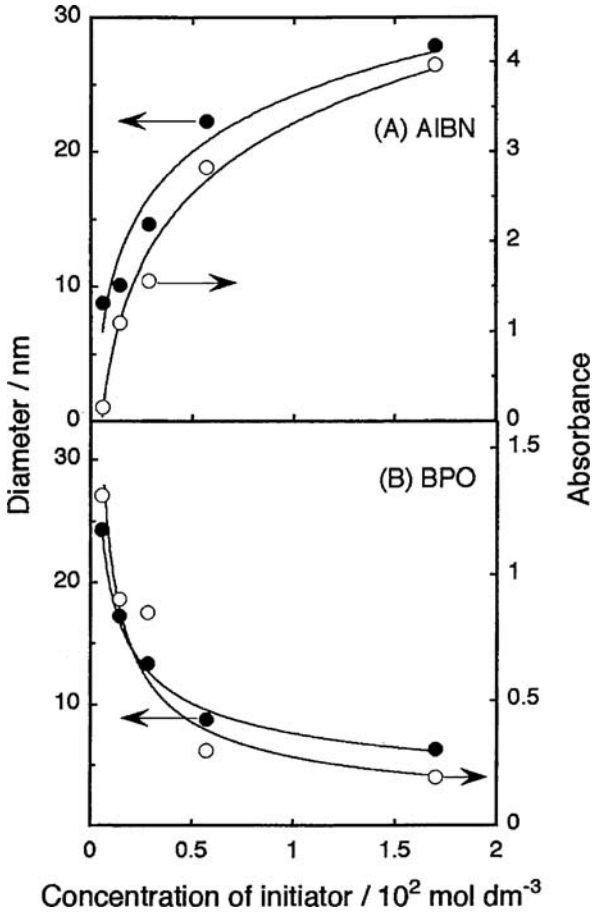

Figure 3.23. Relationships between the average diameter of Ag particles (closed circle), and peak intensities of surface plasmon absorption of Ag clusters at ca. 420 nm (open circle), and the initiator concentration. [N. Yanagihara, K. Uchida, M. Wakabayashi, Y. Uetake, and T. Hara, *Langmuir* **15**, 3038 (1999).]

The type and concentration of polymerization initiators were found to have significant effects on size and size distribution of the grown metallic nanoparticles as shown in Fig. 3.23.[160] Although all the other experimental conditions were kept the same, the variation of the concentration and the type of the polymer radicals demonstrated distinct influences on the Ag particle sizes. Under a steady-state condition as

applied in the above synthesis of Ag-PMMA composite, the concentration of the polymer radicals is proportional to the initial concentration of initiators.[163] Therefore, an increased concentration of polymer initiators are expected to result in an increased amount of polymer chain radicals, which would promote the reduction of metal ions and thus produce more metal atoms for nucleation (a higher concentration or supersaturation). Early discussion (Eqs. (3.5) and (3.9)) indicates that a higher supersaturation permits a smaller size but generates a larger number of nuclei. This explains the results presented in Fig. 3.22(b), which shows that the Ag nanoparticle size decreases with an increased concentration of BPO initiator. However, Fig. 3.22(a) shows an opposite relationship that the nanoparticle size increases with an increased concentration of AIBN initiator. A possible explanation for the results is that benzoyloxy radicals have an oxidation power against metal ions, whereas the isobutyronitrile radicals do not.[163,164] Furthermore, it was found that a high concentration of metal atoms would favor the surface process limited growth, leading to a wide size distribution.

Metallic nanoparticles were also prepared through precipitation or crystallization by annealing amorphous metal alloys at elevated temperatures.[165,166] Superparamagnetic nanocrystalline $Fe_{63.5}Cr_{10}Si_{13.5}B_9Cu_1Nb_3$ in the form of a ribbon of ~10 mm wide and ~25 μm thick was made by a melt spinning technique, followed an annealing at elevated temperatures in argon.[167] The average grain size was found to range from ~5 nm to ~10 nm and to increase with the annealing temperature ranging from 775 K to 850 K.[167]

3.3. Nanoparticles Through Heterogeneous Nucleation

3.3.1. *Fundamentals of heterogeneous nucleation*

When a new phase forms on a surface of another materials, the process is called heterogeneous nucleation. Let us consider a heterogeneous nucleation process on a planar solid substrate. Assuming growth species in the vapor phase impinge on the substrate surface, these growth species diffuse and aggregate to form a nucleus with a cap shape as illustrated in Fig. 3.24. Similar to homogeneous nucleation, there is a decrease in the

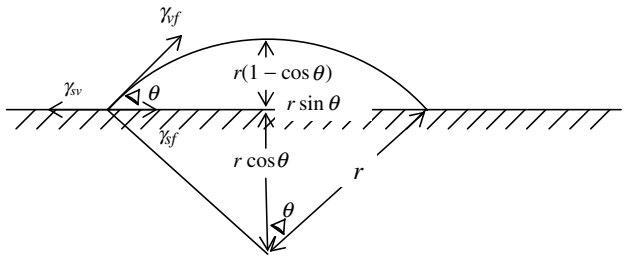

Figure 3.24. Schematic illustrating heterogeneous nucleation process with all related surface energy in equilibrium.

Gibbs free energy and an increase in surface or interface energy. The total change of the chemical energy, ΔG, associated with the formation of this nucleus is given by:

$$\Delta G = a_3 r^3 \Delta\mu_v + a_1 r^2 \gamma_{vf} + a_2 r^2 \gamma_{fs} - a_2 r^2 \gamma_{sv}, \tag{3.43}$$

where r is the mean dimension of the nucleus, $\Delta\mu_v$ is the change of Gibbs free energy per unit volume, γ_{vf}, γ_{fs}, and γ_{sv} are the surface or interface energy of vapor–nucleus, nucleus–substrate, and substrate–vapor interfaces, respectively. Respective geometric constants are given by:

$$a_1 = 2\pi(1-\cos\theta), \tag{3.44}$$

$$a_2 = \pi \sin^2\theta, \tag{3.45}$$

$$a_3 = 3\pi(2 - 3\cos\theta + \cos^2\theta), \tag{3.46}$$

where θ is the contact angle, which is dependent only on the surface properties of the surfaces or interfaces involved, and defined by Young's equation:

$$\gamma_{sv} = \gamma_{fs} + \gamma_{vf}\cos\theta. \tag{3.47}$$

Similar to homogeneous nucleation, the formation of new phase results in a reduction of the volume free energy, but an increase in the total surface energy. The nucleus is stable only when its size is larger than the critical size, r^*:

$$r^* = \frac{-2(a_1\gamma_{vf} + a_2\gamma_{fs} - a_2\gamma_{sv})}{3a_3\Delta G_v} \tag{3.48}$$

and the critical energy barrier, ΔG^*, is given by:

$$\Delta G^* = \frac{4(a_1\gamma_{vf} + a_2\gamma_{fs} - a_2\gamma_{sv})^3}{27{a_3}^2\Delta G_v} \tag{3.49}$$

Substituting all the geometric constants, we get:

$$r^* = \frac{2\pi\gamma_{vf}}{\Delta G_v}\left(\frac{\sin^2\theta\cos\theta + 2\cos\theta - 2}{2 - 3\cos\theta + \cos^3\theta}\right)$$
$$\Delta G^* = \left\{\frac{16\pi\gamma_{vf}}{3(\Delta G_v)^2}\right\}\left\{\frac{(2 - 3\cos\theta + \cos^3\theta)}{4}\right\} \tag{3.50}$$

Comparing this equation with Eq. (3.6), one can see that the first term is the value of the critical energy barrier for homogeneous nucleation, whereas the second term is a wetting factor. When the contact angle is 180°, i.e., the new phase does not wet on substrate at all, the wetting factor equals to one and the critical energy barrier becomes the same as that of homogeneous nucleation. In the case of the contact angle less than 180°, the energy barrier for heterogeneous nucleation is always smaller than that of homogeneous nucleation, which explains the fact that heterogeneous nucleation is easier than homogeneous nucleation in most cases. When the contact angle is 0°, the wetting factor will be zero and there is no energy barrier for the formation of new phase. One example of such cases is that deposit is the same material as the substrate.

For the synthesis of nanoparticles or quantum dots on substrates, $\theta > 0$ is required and the Young's equation becomes:

$$\gamma_{sv} < \gamma_{fs} + \gamma_{vf}\,. \tag{3.51}$$

Such heterogeneous nucleation is generally referred to as island (or Volmer–Weber) growth in the thin films community.[143] Other two nucleation-modes are layer (or Frank–van der Merwe) and island-layer (or Stranski–Krastanov) growth. Detailed discussion will be presented in Chapter 5.

3.3.2. *Synthesis of nanoparticles*

Various methods have been proposed to generate homogeneous surface defects to act as nucleation centers, including thermal oxidation,[168]

sputtering and thermal oxidation,[169] and Ar plasma and ulterior thermal oxidation.[170] Evaporated metals such as silver and gold tend to form small particles on highly oriented pyrolitic graphite (HOPG) substrate.[171] Such formed metal nanoparticles were found closely associated with surface defects.[169,171,172] When edges are the only defects on substrate surfaces, the particles concentrated only around these edges. For example, metal atoms on the substrates would diffuse and form particles concentrated at the step edges, since step edges on a substrate are preferred nucleation sites due to its high-energy state. However, when other defects such as pit holes, the nanoparticles were found to distributed all over the substrate surfaces as demonstrated in Fig. 3.25.[172]

Nickel nanoparticles of diameters ranging from 20 to 600 nm with a narrow size distribution on HOPG substrate were synthesized using a hydrogen coevolution electrochemical deposition.[173] The chemicals used in the synthesis are $Ni(NO_3)_2.6H_2O$, NH_4Cl, NaCl, and NH_4OH and the aqueous solution was kept at a pH of 8.3 during the synthesis.

GaAs nanoparticles in size range from 2.5 to 60 nm is grown on high surface area amorphous silica spheres of ~100 nm by molecular beam epitaxy (MBE).[174] The synthesis of GaAs nanoparticles takes place at ~580°C under conditions typically used for the growth of high quality epitaxial films. GaAs nanoparticles larger than 3.5 nm have a good crystalline order with a lattice constant equal to that of bulk material. Such prepared GaAs nanoparticles are covered with a shell of native oxides, Ga_2O_3 and As_2O_3, of 1.0 to 1.5 nm in thickness.

It should be noted that the formation of nanoparticles through heterogeneous nucleation is different from the synthesis by vapor phase reaction (Sec. 3.2.6). For homogeneous nucleation in vapor phase, particles are first formed in the vapor phase and then deposit onto substrate surfaces, whereas for heterogeneous nucleation, growth species impinge onto and form nuclei on substrate surfaces.

3.4. Kinetically Confined Synthesis of Nanoparticles

Kinetically controlled growth is to spatially confine the growth so that the growth stops when the limited amount of source materials is consumed or the available space is filled up. Many spatial confinements have been established for the synthesis of nanoparticles. In general, spatial confinement can

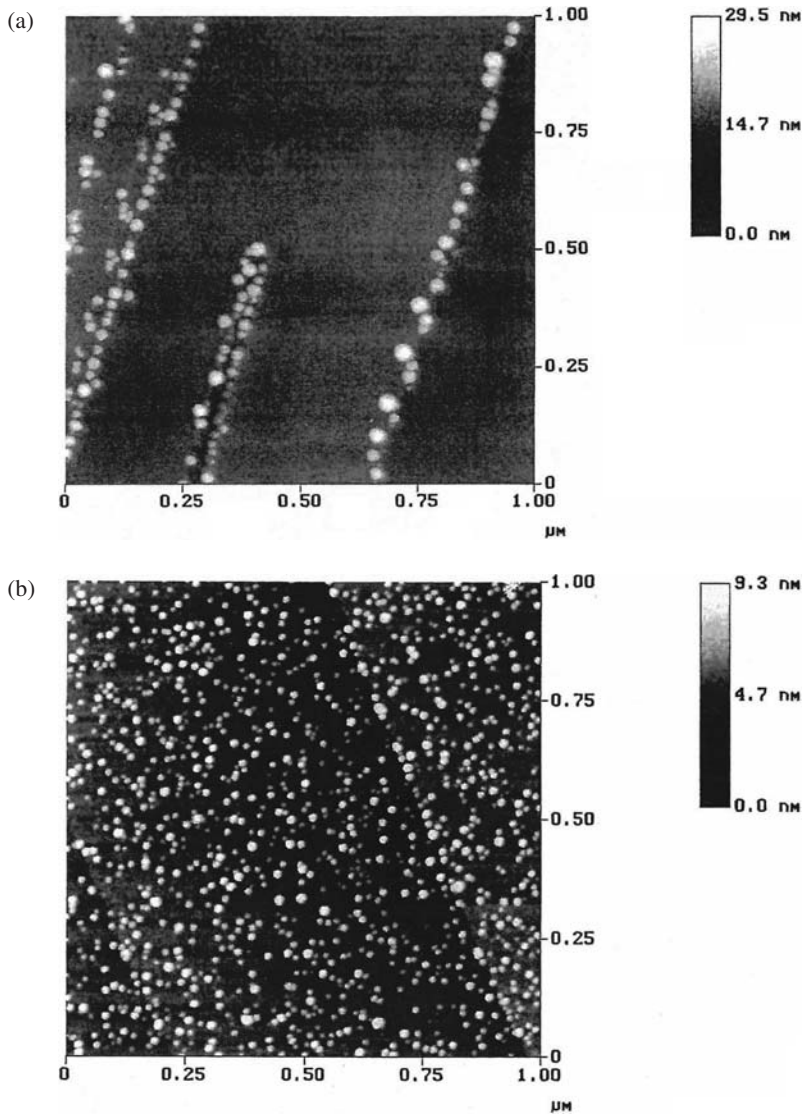

Figure 3.25. Scanning force microscopy images of silver nanoparticles on HOPG-298 graphite substrates: (a) growth occurs only at the edge defects in the original substrate and (b) growth occurs wherever surface defects are present. [A. Stabel, K. Eichhorst-Gerner, J.P. Rabe, and A.R. González-Elipe, *Langmuir* **14**, 7324 (1998).]

be divided into several groups: (1) liquid droplets in gas phase including aerosol synthesis and spray pyrolysis, (2) liquid droplets in liquid, such as micelle microemulsion synthesis, (3) template-based synthesis, and (4) self-terminating synthesis. All these methods will be briefly discussed in this section.

3.4.1. *Synthesis inside micelles or using microemulsions*

The synthesis of nanoparticles can be achieved by confining the reaction in a restricted space. This method is exemplified by the synthesis of nanoparticles inside micelles or in microemulsion. A microemulsion is a thermodynamically stable dispersion of two immiscible liquids with the assistance of an emulsifier or surfactant.[175] For example, water-in-oil (w/o) microemulsions appear when water is dispersed homogenously in an organic media. The w/o microemulsions have attracted considerable interest due to their application in the preparation of metallic nanoparticles,[176,177] semiconductor quantum dots[178] and polymeric nanoparticles.[179] Microemulsion-based method can be used to synthesize micro-homogeneous products with desired stoichiometry, whereas expensive or special instruments are not needed.

Reverse micelles (microemulsion with $[H_2O]/[\text{surfactant}] < 15$) are utilized as templates to prepare metallic nanoparticles of Pt, Rh, Pd and Ir as early as in 1982. The factors which influence the morphology and size of the obtained metal nanoparticle have been discussed by Capek.[180] Metallic Pd nanoparticles can transform from spherical nanoparticles to worm-like nanostructures by increasing the water content.[181] It has been claimed that the shape and size of copper nanoparticles are affected by water content, capping agent, and concentration of reducing agent.[182] The microemulsion method can also be used to synthesize bimetallic alloy nanoparticles such as Fe/Pt[183] and Cu/Ni[184] which show improved properties compared to their counterparts. Moreover, with the assitance of microemulsion, various oxide nanoparticles can be prepared, including simple binary oxides such as CeO_2,[185] ZrO_2,[185] Fe_2O_3[186] and complex ternary oxide such as $BaTiO_3$,[185] $SrZrO_3$,[185] $LaMnO_3$.[187] It should be noted that ultra-small tungsten oxides with diameters of around 5 nm can be

synthesized using microemulsion-assisted method and the reaction temperature is lower than that used in the conventional methods.[188]

In micelle synthesis, reactions proceed among the reactants that are available only inside the micelle and the particle stops growing when the reactants are consumed. The formation of micelles will be discussed in detail late in Chapter 6; however, a brief description of the formation of micelles is given below. When surfactants or block polymers, typically consisting of two parts: one hydrophilic and another hydrophobic, are dissolved into a solvent, they preferentially self-assemble at air/aqueous solution or hydrocarbon/aqueous solution interfaces. The hydrophilic part is turned towards the aqueous solution. When the concentration of the surfactants or block polymers exceeds a critical level, they self-assemble in such a way to form micelles. Surfactants or block polymers will reside at the interface separating hydrocarbon and aqueous solutions. A microemulsion is a dispersion of fine liquid droplets of an organic solution in an aqueous solution. Such a microemulsion system can be used for the synthesis of nanoparticles. The chemical reactions can take place either at the interfaces between the organic droplets and aqueous solution, when reactants are introduced separately into two nonmixable solutions, or inside the organic droplets when all the reactants are dissolved into the organic droplets.

Let us take the work by Steigerwald *et al.*[87] on the synthesis of CdSe nanoparticles using organometallic reagents in inverse micellar solution as an example to illustrate a typical synthesis process. The surfactant bis(2-ethylhexyl) sulfosuccinate (aerosol-OT; AOT) of 33.3g is dissolved in heptane (1300 mL), and then deoxygenated water (4.3 mL) is added. The mixture is stirred magnetically until the mixture becomes homogeneous, which gives a microemulsion with the ratio $W = [H_2O]/[AOT] = 3.2$. 1.12 mL of 1.0 M Cd^{2+} solution, prepared from $Cd(ClO_4)_2 \cdot 6H_2O$ and deoxygenated water, is added to the above microemulsion. Stirring gives an optically homogeneous microemulsion with $W = 4.0$. A solution of bis(trimethylsily)selenium, $Se(TMS)_2$ (210 μL) in heptane (50 mL) is added quickly to the microemulsion via syringe. A color develops throughout the homogeneous microemulsion as the semiconductor particles form. Under otherwise similar processing conditions, the ratio of $W = [H_2O]/[AOT]$ controls the size of CdSe crystallites. The same results

were reported in the formation of colloidal crystallites from ionic reagents.[189,190]

The surface of the semiconductor nanoparticles prepared in inverse micellar solution can be further modified, and in general, surface modification is achieved by introducing silylorganoselenides, which react quickly with metal salts to form metal selenium covalent bonds.[87,191] For example, the surfactant stabilized CdSe is first coated with Cd^{2+} by the addition of 0.5 mL of 1.0 M Cd^{2+} solution and then with 350 μL of phenyl(trimethylsilyl)selenium, PhSeTMS in 50 mL of heptane. The mixture becomes cloudy and the colored precipitate is collected either by centrifugation or filtration. In this process, a Cd-rich surface is first generated on the CdSe nanocrystallites, and then reacts with PhSeTMS to form a layer of phenyl ligands which form covalent bonds with and cover the CdSe surface.[87]

Various monodispersed polymer particles can be prepared by carefully controlled emulsion polymerizations.[192–194] Typically a water-soluble polymerization initiator and a surfactant are added into a mixture of water and monomer. The hydrophobic monomer molecules form large droplets, typically 0.5 to 10 μm in diameter, which are stabilized by the surfactant molecules whose hydrophilic ends point outward and whose hydrophobic ends point inward toward the monomer droplet. The concentration of micelles, typically 10^{18} per mL, is far larger than that of the monomer droplets, 10^{10}–10^{11} per mL. Polymerization-initiators enter both monomer droplets and micelles. Polymerization proceeds in both monomer droplets and micelles with monomers transferred from monomer droplets. The resulting polymer particles are typically between 50 nm and 0.2 μm in diameter.[192] Such prepared polymer colloids were found to have exceedingly narrow size distribution and spherical shape.[195,196]

3.4.2. *Aerosol synthesis*

The formation of nanoparticles by aerosol method differs from other methods in several aspects. First of all, aerosol method can be considered as a top-down approach as compared with other methods, which have a bottom-up approach. Secondly, nanoparticles can be polycrystalline as

compared with either single crystalline or amorphous structure of nanoparticles prepared by other methods. Thirdly, the nanoparticles prepared need to be collected and redispersed for many applications. In this method, a liquid precursor is first prepared. The precursor can be a simple mixture solution of desired constituent elements or a colloidal dispersion. Such a liquid precursor is then mistified to make a liquid aerosol, i.e., a dispersion of uniform droplets of liquid in a gas, which may simply solidified through evaporation of solvent or further react with the chemicals that are present in the gas. The resulting particles are spherical and their size is determined by the size of the initial liquid droplets and concentration of the solid. Aerosols can be relatively easily produced by sonication or spinning.[197] For example, TiO_2 particles can be produced from $TiCl_4$ or titanium alkoxide aerosols.[198] First amorphous spherical titania particles are formed, and then converted to anatase crystalline when calcined at elevated temperatures. Rutile phase is obtained when the powders are heated at 900°C. Following the same procedure with Al-2'-butoxide droplets, spherical alumina particles can be produced.[199]

The aerosol technique has also been used in the preparation of polymer colloids. The starting materials are droplets of organic monomers that can be either polymerized in contact with an initiator in gaseous state,[200] or copolymerized with another organic reactant.[201] For example colloidal particles of poly(p-tertiarybutylstyrene) were prepared by polymerizing monomer droplets dispersed in helium gas with trifluoromethanesulfonic acid vapor, which acted as the polymerization initiator.[200] Polymer particles of styrene and divinylbenzene were synthesized through copolymerization between two monomers: styrene and divinylbenzene.[201] It should be noted that the polymer particles formed using aerosol synthesis are large particles, with diameters ranging from ~1 to 20 micron meters.

3.4.3. *Growth termination*

In the synthesis of nanoparticles, the size can be controlled by so-called growth termination. The approach is conceptually straightforward. When organic components or alien ions are attached to the growth surface strongly so that all the available growth sites are occupied, growth process stops. Herron and coworkers[202] synthesized colloidal particles of CdS

based on the competitive growth and termination of CdS species in the presence of thiophenol surface capping agents. Cadmium acetate, thiophenol, and anhydrous sodium sulfide were used for the synthesis and all the synthetic procedures and manipulations were carried out in a dry-box filled with nitrogen. Three stock solutions were prepared: (A) cadmium acetate dissolved into methanol, [Cd] = 0.1 M, (B) sodium sulfide in a mixture of water and methanol in 1:1 volume ratio, $[S^{2-}] = 0.1$ M, and (C) thiophenol in methanol, [PhSH] = 0.2 M. Stock solutions B and C were first thoroughly mixed and then stock solution A was added under stirring in an overall volume ratio of A:B:C = 2:1:1. The solution was stirred for 15 min, filtered, and suction dried through a filter by nitrogen. Such prepared CdS particles were crystalline and XRD spectra matched with that of bulk sphalerite CdS. The surface of the CdS particles was capped with thiophenol molecules as schematically illustrated in Fig. 3.26.[202] CdS particle sizes varied with the relative ratio of sulfide to thiophenol and ranged from less than 1.5 nm to ~3.5 nm. It was clearly demonstrated that an increasing amount of capping molecules relative to sulfide precursor resulted in a reduced particle size. Therefore, the size of these nanoparticles could be conveniently controlled by adjusting the relative concentrations of capping molecules and precursors. Similar synthetic approach is applicable to the formation of metal oxide nanoparticles. For example, crystalline tetragonal ZrO_2 nanoparticles of 2 nm in diameter is formed by hydrolysis of acac-modified zirconium propoxide in the presence of para-toluene sulfonic acid and aging at 60–80°C.[203]

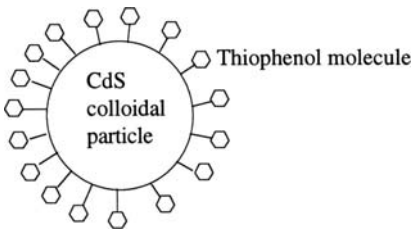

Figure 3.26. Termination growth for the synthesis of nanoparticles. When organic components occupy all the surface growth sites, growth of nanoparticle stops. The final size of grown nanoparticles can be controlled by the concentration of organic ligands introduced to the system. [N. Herron, Y. Wang, and H. Eckert, *J. Am. Chem. Soc*. **112**, 1322 (1990).]

3.4.4. *Spray pyrolysis*

Spray pyrolysis is basically a solution process and has been widely used in the preparation of metal and metal oxide powders.[204,205] The process can be simply described as converting microsized liquid droplets of precursor or precursor mixture into solid particles through heating. In practice, spray pyrolysis involves several steps: (1) generating microsized droplets of liquid precursor or precursor solution, (2) evaporation of solvent, (3) condensation of solute, (4) decomposition and reaction of solute, and (5) sintering of solid particles.

Kieda and Messing[206] reported the production of silver particles using precursor solutions of Ag_2CO_3, Ag_2O and $AgNO_3$ with NH_4HCO_3 at temperatures of 400°C or less. It was recognized that the ability of silver ions to form the ammine complexes plays a very important role in the production of nanoparticles in this low temperature spray pyrolysis. It was postulated that such a process would be applicable for most transition metals such as Cu, Ni, Zn, ions of which can form complexes with ammines.

Brennan *et al*.[207] prepared nanometer-sized particles of CdSe starting from either $Cd(SePh)_2$ or $[Cd(SePh)_2]_2[Et_2PCH_2CH_2PEt_2]$ through a mild solid-state pyrolysis *in vacuo* at temperatures ranging from 320 to 400°C for 24 h. Analogue process was used to produce nanoparticles of ZnS and CdS,[208] and CdTe and HgTe.[209]

Oxide nanoparticles can also be prepared by spray pyrolysis. Kang *et al*.[210] made Y_2O_3 nanoparticles doped with europium by a combination of sol–gel processing and spray pyrolysis. Colloidal solution was prepared using urea as a reduction reagent and spray pyrolysis was carried at about 1300°C. Nanoparticles were found to exhibit smooth surface, spherical shape, and hollow structure.

3.4.5. *Template-based synthesis*

Iron oxide, Fe_3O_4 nanoparticles dispersed in a solid polymer matrix can be synthesized by infiltration of iron chloride solution.[211] The polymer matrices are cation exchange resins, which are formed by beads of 100–300 μm in diameter and contain micropores. The iron oxide nanoparticle synthesis

is performed in nitrogen by dispersing the resin in an iron chloride solution. Matrix cations, Na^+ or H^+, are exchanged with Fe^{2+} and Fe^{3+}. The exchange is followed by hydrolysis and polymerization in an alkaline medium at 65°C with the formation of Fe_3O_4 nanoparticles within the resin macropores. The process is repeated to increase the load of Fe_3O_4 and thus the size of nanoparticles. Regularly shaped spheres of Fe_3O_4 with diameters ranging from 3 to 15 nm are prepared. CdSe nanoparticles have also been synthesized using zeolites as templates[212] and ZnS nanoparticles in silicate glasses.[213] Templates can also be used as a shadow mask for the synthesis of nanoparticles by gas deposition. For example, ordered arrays of multiple metallic nanoparticles on silicon substrates were deposited by evaporation using anodic porous alumina membranes as masks.[214]

3.5. Epitaxial Core–Shell Nanoparticles

Nanoparticles have been subjected to a variety of surface engineering for various applications including self-assembly of organic components and bioactive species, and dielectric–metal core–shell nanostructures. This topic deserves special attention and will be discussed in detail in Chapter 6. However, the semiconductor–semiconductor core–shell structures will be discussed below, since such core–shell structures grow epitaxially and the shell can be considered as an extension of core structure with different chemical compositions. In addition, the growth of core and shell in these systems are very closely related.

Semiconductor nanoparticles can have quantum effects and have high emission yields across the visible and near infrared (NIR) spectrum. The surface of such nanoparticles or quantum dots largely determines the quantum yield and emission life-time of the bandgap luminescence. High luminescence yields are achieved by the use of surface passivation to reduce the non-radiative surface recombination of charge carriers. Two methods of passivation are commonly employed. One is through so-called bandgap engineering, whereby a larger bandgap semiconductor with good lattice mismatch is epitaxially deposited onto the core.[215] Another method is to adsorb Lewis bases onto the surface.[216,217] One example of the latter is otylamine used to passivate the surface of CdSe and CdSe/ZnS quantum dots.[218]

For the growth of a layer of larger bandgap semiconductor on the surface of a nanoparticle, the growth condition must be controlled such that no homogeneous nucleation would occur, but only a growth proceeds on the surface of the nanoparticles. Therefore, the concentration of the growth species needs to be controlled such that the supersaturation is not high enough for nucleation, but high enough for growth. There are two approaches applied to control the supersaturation of growth species. One is by the drop wise addition of growth precursor solution into the reaction mixture, which consists of grown nanoparticles (cores). Another method is to vary the growth temperatures. For example, in the synthesis of CdSe/ZnS core/shell nanostructures, the temperatures at which each individual size of nanoparticles was overcoated are as follows: 140°C for 2.3 and 3.0 nm diameters, 160°C for 3.5 nm, 180°C for 4.0 nm, 200°C for 4.8 nm, and 220°C for 5.5 nm.[219] Lower temperature is required for the growth on smaller nanoparticles, since the solubility and the supersaturation depends on the surface curvature as discussed in the previous chapter. Furthermore, the association between the surface atoms or ions of the nanoparticles (cores) and the capping materials should not be too strong, so that the growth species can displace the capping molecules or insert between the surface atom and the capping molecules.

In the following, a few examples will be used to further illustrate the general approach in fabricating core–shell nanostructures. First, let us look at the preparation of ZnS-capped CdSe nanocrystals.[215] The CdSe nanocrystallites are prepared by method described earlier in Sec. 3.2.4.[86] The Zn and S stock solution was prepared with 0.52 mL of bis-trimethylsilyl sulfide, $(TMS)_2S$ (0.0025 mol) in 4.5 mL of TOP, adding 3.5 mL of dimethylzinc, Me_2Zn solution (0.0035 mol), and diluting with 16 mL of TOP in a nitrogen filled dry-box. When the TOP capped CdSe colloidal dispersion is prepared and cooled to ~300°C, the Zn/S/TOP solution was injected into CdSe colloidal dispersion five times at approximately 20 s intervals. A total mole ratio of injected reagents was 1:4 Cd/Se:Zn/S. Upon cooling the reaction mixture was stirred at 100°C for 1 h. A layer of ZnS of ~0.6 nm is coated onto the surface of CdSe nanoparticles as supported by X-ray photoelectron spectroscopy and transmission electron microscopy. Figure 3.27 shows the TEM picture of ZnS-capped CdSe nanocrystals.[215]

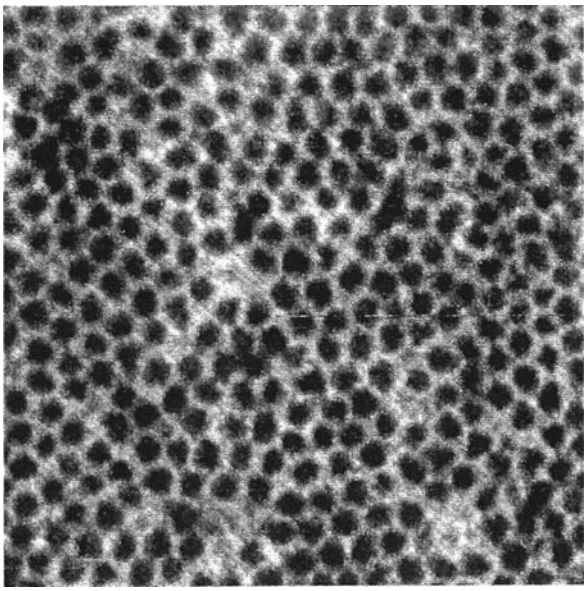

Figure 3.27. TEM image of ZnS-capped CdSe nanocrystals. This picture is 95×95 nm. [M.A. Hines and P. Guyot-Sionnest, *J. Phys. Chem.* **100**, 468 (1996).]

The epitaxial growth of shell material on the core nanocrystallites can eliminate both the anionic and cationic surface dangling bonds, and also generate a new nanocrystal system, as demonstrated by Peng *et al*.[220] The wurtzite CdSe/CdS structure is ideal in many aspects. The lattice mismatch of 3.9% is small enough to allow heteroepitaxial growth, while still large enough to prevent alloying, and the difference in bandgaps is large enough for shell growth to increase the quantum yield and the stability of the cores. The synthesis procedure of CdSe/CdS core/shell structures is described below.[220] First stock solution for CdSe nanocrystal synthesis was prepared. CdSe stock solution was made by adding the desired amount of $Cd(CH_3)_2$ to a solution of Se powder dissolved in tributylphophine (TBP) in a dry-box under nitrogen, with the Cd:Se molar ratio kept as 1:0.7 or 1:0.9. TOPO, used as a high-boiling point solvent as well as stabilizer, was heat to 360°C under argon before a stock solution was quickly injected. The reaction was either stopped immediately by quick removal of the heating or allowed to continue after lowering the

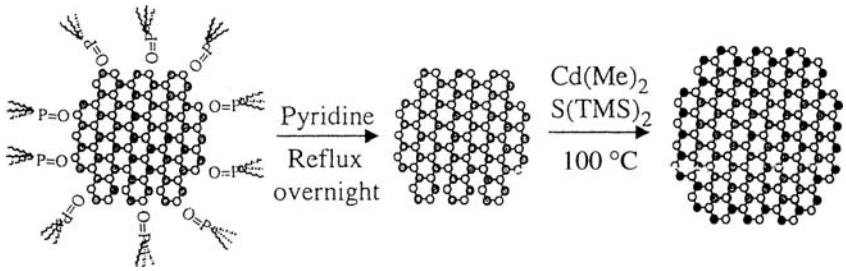

Figure 3.28. Schematic synthesis of CdSe/CdS core/shell nanocrystals [X. Peng, M.C. Schlamp, A.V. Kadavanich, and A.P. Alivisatos, *J. Am. Chem. Soc*. **119**, 7019 (1997).]

temperature to 300°C. Nanocrystals were precipitated by the addition of methanol to the cooled, room temperature reaction mixture. After centrifugation and drying under nitrogen, CdSe nanocrystals capped with TOPO and of 3.5 nm in diameter were obtained. For the shell growth, the above CdSe nanocrystals were dissolved into anhydrous pyridine and refluxed over night under argon. CdS stock solution, made by adding $(TMS)_2S$ to a solution of $Cd(CH_3)_2$ dissolved in TBP under nitrogen with a Cd:S molar ratio of 1:2.1, was added drop wise (one drop per second) to the reaction solution at 100°C. Stopping the addition of CdS stock solution and removing of the heating source would terminate the shell growth. Dodecylamine was added to the reaction solution at room temperature until the nanocrystals precipitated. When CdSe nanoparticle is refluxed in pyridine overnight, TOPO could be almost completely removed from CdSe nanocrystals without affecting the nanocrystal structure. Pyridine displaces TOPO and forms a weak bond to a surface Cd atom, providing simultaneous chemical stability and access to the surface, permitting the growth of CdS shell to CdSe core. This reaction is schematically shown in Fig. 3.28.[220]

3.6. Summary

The preparation of monodispersed nanoparticles can be achieved through many different approaches, either homogeneous or heterogeneous nucleation, in gaseous, liquid, or solid medium. There are some common fundamentals for the synthesis of nanoparticles with monodispersion.

(1) Temporal nucleation, i.e., nucleation occurs in a very short time. Such a temporal nucleation is achieved through generating an abrupt supersaturation. Introduction of monosized seeds for heterogeneous nucleation and growth is another approach. (2) Subsequent growth needs to be diffusion-controlled. This is achieved through introducing a diffusion barrier, such as a polymer monolayer on the growth surface, using a low concentration of growth species, or slowly generating growth species. (3) Ostwald ripening is often used to further narrow the size distribution. (4) Size selective precipitation is applied to further separate large particles from small ones, though it is done after the synthesis. In contrast to spontaneous growth of monodispersed nanoparticles, spatial confinement is also applied to the synthesis of nanoparticles. The technical approach here is very straightforward: only a certain amount of growth species or a limited space is available for the formation of individual nanoparticles.

References

1. E.H.C. Parker (ed.), The *Technology and Physics of Molecular Beam Epitaxy*, Plenum, New York, 1985.
2. J.J. Jewell, J.P. Harbison, A. Scherer, Y.H. Lee, and L.T. Florez, *IEEE J. Quantum Electron.* **27**, 1332 (1991).
3. M. Haruta and B. Delmon, *J. Chim. Phys.* **83**, 859 (1986).
4. A.E. Nielsen, *Kinetic of Precipitation*, MacMillan, *New York,* 1964.
5. R. Williams, P.M. Yocom, and F.S. Stofko, *J. Colloid Interf. Sci.* **106**, 388 (1985).
6. A. Henglein, *Chem. Rev.* **89**, 1861 (1989).
7. Z.L. Wang, *Adv. Mater*. **10**, 13 (1998).
8. G. Schmid, *Chem. Rev.* **92**, 1709 (1992).
9. G. Schmid (ed.), *Clusters and Colloids*, VCH, New York, 1994.
10. G. Schon and U. Simon, *Colloid Polym Sci.* **273**, 101 (1995).
11. M. Faraday, *Phil. Trans*. **147**, 145 (1857).
12. J. Turkevich, J. Hillier, and P.C. Stevenson, Discuss. *Faraday Soc.* **11**, 55 (1951).
13. J. Turkevich, *Gold Bull*. **18**, 86 (1985).
14. H. Hirai, Y. Nakao, N. Toshima, and K. Adachi, *Chem. Lett*. 905 (1976).
15. H. Hirai, Y. Nakao, and N. Toshima, J. Macromol, *Sci. Chem*. **A12**, 1117 (1978).

16. A. Henglein, B.G. Ershov, and M. Malow, *J. Phys. Chem.* **99**, 14129 (1995).
17. J. Turkevich and G. Kim, *Science* **169**, 873 (1970).
18. J. Turkevich, K. Aika, L.L. Ban, I. Okura, and S. Namba, *J. Res. Inst. Catal.* **24**, 54 (1976).
19. L.D. Rampino and F.F. Nord, *J. Am. Chem. Soc.* **63**, 2745 (1941).
20. F.A. Cotton and G. Wilkison, *Advanced Inorganic Chemistry*, 5th edn. John Wiley, New York, 1988.
21. R.A. Salkar, P. Jeevanandam, S.T. Aruna, Y. Koltypin, and A. Gedanken, *J. Mater. Chem.* **9**, 1333 (1999).
22. M. Gutierrez and A. Henglein, *J. Phys. Chem.* **91**, 6687 (1987).
23. M.T. Reetz and W. Helbig, *J. Am. Chem. Soc.* **116**, 7401 (1994).
24. J.A. Becker, R. Schafer, R. Festag, W. Ruland, J.H. Wendorff, J. Pebler, S.A. Quaiser, W. Helbig, and M.T. Reetz, *J. Chem. Phys.* **103**, 2520 (1995).
25. K.H. Lieser, *Angew. Chem. Int. Ed. Engl.* **8**, 188 (1969).
26. V.K. La Mer, *Ind. Eng. Chem. Res.* **44**, 1270 (1952).
27. W.O. Miligan and R.H. Morriss, *J. Am. Chem. Soc.* **86**, 3461 (1964).
28. M.T. Reetz and M. Maase, *Adv. Mater.* **11**, 773 (1999).
29. D.G. Duff, P.P. Edwards, and B.F.G. Johnson, *J. Phys. Chem.* **99**, 15934 (1995).
30. K. Chou and C. Ren, *Mater. Chem. Phys.* **64**, 241 (2000).
31. A. Henglein, *Chem. Mater.* **10**, 444 (1998).
32. T.S. Ahmadi, Z.L. Wang, T.C. Green, A. Henglein, and M.A. El-Sayed, *Science* **272**, 1924 (1996).
33. Y. Yin, Z. Li, Z. Zhong, B. Gates, Y. Xia, and S. Venkateswaran, *J. Mater. Chem.* **12**, 522 (2002).
34. A.G. Ingalls, *Amateur Telescope Making* (*Book One*), Scientific American Inc., New York, p. 101, 1981.
35. P. Toneguzzo, G. Viau, O. Acher, F. Fiévet-Vincent, and F. Fiévet, *Adv. Mater*. **13**, 1032 (1998).
36. Q.A. Pankhurst, J. Connolly, S.K. Jones, J. Dobson, and J. Phys. D: *Appl. Phys*. **36**, R167 (2003).
37. K.M. Nam, J.H. Shim, H. Ki, S. Choi, G. Lee, J. Jang, Y. Jo, M. Jung, H. Song, and J. T. Park, *Angew. Chem. Int. Ed.* **47**, 9504 (2008).
38. C. Desvaux, C. Amiens, P. Fejes, P. Renaud, M. Respaud, P. Lecante, E. Snoeck, and B. Chaudret, *Nat Mater* **4**, 750 (2005).
39. Y. Bao, K.M. Krishnan *J. Magn.* Magn. *Mater.* **15**, 293 (2005).

40. W-r. Lee, M.G. Kim, J-r. Choi, J-I. Park, S.J. Ko, S.J. Oh, and J. Cheon, *J. Am. Chem. Soc.* **127 (46)**, 16090 (2005).
41. H. Kim, M. Achermann, L.P. Balet, J.A. Hollingsworth, and V.I. Klimov, *J. Am. Chem. Soc.* **127**, 544 (2005).
42. M.L. Vadala, M.A. Zalich, D.B. Fulks, T.G.S. Pierre, J.P. Dailey, J.S. Riffle, and *J. Magn. Magn. Mater.* **162**, 293 (2005).
43. G.S. Chaubey, C. Barcena, N. Poudyal, C. Rong, J. Gao, S. Sun, and J. Ping. Liu, *J. Am. Chem. Soc.* **129**, 7214 (2007).
44. W.S. Seo, J.H. Lee, Z. Sun, Y. Suzuki, D. Mann, Z. Liu, M. Terashima, P. Yang, M.V. Mcconnell, D.G. Nishimura, and H. Dai, *Nat. Mater.* **5**, 971 (2006).
45. Z. Turgut, J.H. Scott, M.Q. Huang, S.A. Majetich, and M.E. McHenry, *J. Appl. Phys.* **83**, 6468 (1998).
46. J. Bai and J.-P. Wang, *Appl. Phys. Lett.* **87**, 152502 (2005).
47. L.R. Hirsch, R.J. Stafford, J.A Bankson, S.R. Sershen, B. Rivera, R.E. Price, J.D. Hazle, N.J. Halas, and J.L. West, *Proc. Natl. Acad. Sci. USA* **100**, 13549 (2003).
48. X. Huang, I.H. El-Sayed, W. Qian, and M.A. El-Sayed, *J. Am. Chem. Soc.* **128**, 2115 (2006).
49. C.-C. Chen, Y.-P. Lin, C.-W. Wang, H.-C. Tzeng, C.-H. Wu, Y.-C. Chen, C.-P. Chen, L.-C. Chen, and Y.-C. Wu, *J. Am. Chem. Soc.* **128**, 3709 (2006).
50. N.W.S. Kam, M. O'Connell, J.A. Wisdom, and H. Dai, *Proc. Natl. Acad.Sci.* USA. **102**, 11600 (2005).
51. S. Peng, J. Xie, and S. Sun, *J. Solid State Chem.* **181 (7)**, 1560 (2008).
52. S. Sun, H. Zeng, D.B. Robinson, S. Raoux, P.M. Rice, S.X. Wang, and G. Li, *J. Am. Chem. Soc.* **126**, 273 (2004).
53. A.R. West, *Basic Solid State Chemistry*, John Wiley and Sons: New York, 356–359 (1988).
54. R.C. O'Handley, *Modern Magnetic Materials — Principles and Applications*, John Wiley and Sons: New York, 126–132 (2000).
55. S. Peng, C. Wang, J. Xie, and S. Sun, *J. Am. Chem. Soc.* **128**, 10676 (2006).
56. Q.A. Pankhurst, J. Connolly, S.K. Jones, and J. Dobson, *J. Phys. D: Appl. Phys.* **36**, 167 (2003).
57. C.H. Griffiths, M.P. O'Horo, and T.W. Smith, *J. Appl. Phys.* **50**, 7108 (1979).

58. J. van Wonterghem, S. Mørup, S.W. Charles, and S. Wells, Villadsen, *J. Phys. Rev. Lett.* **55**, 410 (1985).
59. K.S. Suslick, M. Fang, and T. Hyeon, *J. Am. Chem. Soc.* **118**, 11960 (1996).
60. S.-J. Park, S. Kim, S. Lee, Z.G. Khim, K. Char, and T. Hyeon, *J. Am. Chem. Soc.* **122**, 8581 (2000).
61. D. Farrell, S. A. Majetich, and J.P. Wilcoxon, *J. Phys. Chem. B* **107**, 11022 (2003).
62. W. Pei, S. Kakibe, I. Ohta, and M. Takahashi, IEEE Trans. *Magn.* **41**, 3391 (2005).
63. H. Shao, H. Lee, Y. Huang, I. Ko, and C. Kim, IEEE Trans. *Magn.* **41**, 3388 (2005).
64. F. Dumestre, B. Chaudret, C. Amiens, P. Renaud, and P. Fejes, *Science* **303**, 821 (2004).
65. J.P. Wilcoxon and P.P. Provencio, *J. Phys. Chem.* B **103**, 9809 (1999).
66. S. Yamamuro, T. Ando, K. Sumiyama, T. Uchida, and I. Kojima, *Jpn. J. Appl. Phys.* **43**, 4458 (2004).
67. D. Kim, J. Park, K. An, N.-K. Yang, J.-G. Park, and T. Hyeon, *J. Am. Chem. Soc.* **129 (18)**, 5812 (2007).
68. M. Chen, J. Kim, J. P. Liu, H. Fan, and S. Sun, *J. Am. Chem. Soc.* **128**, 7132 (2006).
69. S. Yamamoto, Y. Morimoto, T. Ono, and M. Takano, *Appl. Phys. Lett.* **87**, 032503 (2005).
70. K. Inomata, T. Sawa, and S. Hashimoto, *J. Appl. Phys.* **64**, 2537 (1988).
71. D. Weller and A. Moser, IEEE Trans. *Magn.* **35**, 4423 (1999).
72. M. Hasegawa, K. Uchida, Y. Nozawa, M. Endoh, S. Tanigawa, S.G. Sankar, and M. Tokunaga, *J. Magn. Magn. Mater.* **124**, 325 (1993).
73. T. Budde, H. H. Gatzen, J. Magn. Magn. Mater. **272–276**, 2027 (2004).
74. E. Pina, F.J. Palomares, M.A. Garcia, F. Cebollada, A. de Hoyos, J.J. Romero, A. Hernando, and J.M. Gonzalez, *J. Magn. Magn. Mater.* **290**, 1234 (2005).
75. J. Sayama, K. Mizutani, Y. Yamashita, T. Asahi, and T. Osaka, IEEE Trans. *Magn.* **41**, 3133 (2005).
76. H. Raisigel, O. Cugat, and J. Delamare, Sens. Actuators A **130**, 438 (2006).
77. T. Budde and H.H. Gatzen, *J. Appl. Phys.* **99**, 08N304 (2006).
78. Y. Hou, Z. Xu, S. Peng, C. Rong, J. Liu, and S. Sun, *Adv. Mater.* **19**, 3349 (2007).
79. C.N. Chinnasamy, J.Y. Huang, L.H. Lewis, B. Latha, C. Vittoria, and V.G. Harris, *Appl. Phys. Lett.* **93**, 032505 (2008).

80. M.L. Steigerwald, and L.E. Brus, *Acc. Chem. Res.* **23**, 183 (1990).
81. A.P. Alivisatos, *Science* **271**, 933 (1996).
82. M.G. Bawendi, M.L. Steigerwald, and L.E. Brus, *Annu. Rev. Phys. Chem.* **41**, 477 (1990).
83. Y. Wang, *Acc. Chem. Res.* **24**, 133 (1991).
84. C.B. Murray, C.R. Kagan, and M.G. Bawendi, *Ann. Rev. Mater. Sci.* **30**, 545 (2000).
85. S.A. Majetich and A.C. Carter, *J. Phys. Chem.* **97**, 8727 (1993).
86. C.B. Murray, D.J. Norris, and M.G. Bawendi, *J. Am. Chem. Soc.* **115**, 8706 (1993).
87. M.L. Steigerwald, A.P. Alivisatos, J.M. Gibson, T.D. Harris, R. Kortan, A.J. Muller, A.M. Thayer, T.M. Duncan, D.C. Douglas, and L.E. Brus, *J. Am. Chem. Soc.* **110**, 3046 (1988).
88. S.M. Stuczynski, J.G. Brennan, and M.L. Steigerwald, *Inorg. Chem.* **28**, 4431(1989).
89. L. Spanhel, M. Haase, H. Weller, and A. Henglein, *J. Am. Chem. Soc.* **109**, 5649 (1987).
90. M.G. Bawendi, A. Kortan, M.L. Steigerwald, and L.E. Brus, *J. Chem. Phys.* **91**, 7282 (1989).
91. A.L. Smith, *Particle Growth in Suspensions*, Academic Press, New York, 1983.
92. H. Reiss, *J. Chem. Phys.* **19**, 482 (1951).
93. A.A. Guzelian, J.E.B. Katari, A.V. Kadavanich, U. Banin, K. Hamad, E. Juban, A.P. Alivisatos, R.H. Wolters, C.C. Arnold, and J.R. Heath, *J. Phys. Chem.* **100**, 7212 (1996).
94. A. Guinier, *X-Ray Diffraction*, W.H. Freeman, San Francisco, CA, 1963.
95. O.I. Mićić, J.R. Sprague, C.J. Curtis, K.M. Jones, J.L. Machol, A.J. Nozik, H. Giessen, B. Fluegel, G. Mohs, and N. Peyghambarian, *J. Phys. Chem.* **99**, 7754 (1995).
96. O.I. Mićić, C.J. Curtis, K.M. Jones, J.R. Sprague, and A.J. Nozik, *J. Phys. Chem.* **98**, 4966 (1994).
97. R.L. Wells, M.F. Self, A.T. MaPhail, S.R. Auuchon, R.C. Wandenberg, and J.P. Jasinski, *Organometallics* **12**, 2832 (1993).
98. S.R.Aubuchon, A.T. McPhail, R.L. Wells, J.A. Giambra, and J.R. Bowser, *Chem. Mater.* **6**, 82 (1994).

99. E.K. Byrne, L. Parkanyi, and K.H. Theopold, *Science* **241**, 332 (1988).
100. M.A. Olshavsky, A.N. Goldstein, and A.P. Alivisatos, *J. Am. Chem. Soc.* **112**, 9438 (1990).
101. R.L. Wells, C.G. Pitt, A.T. McPhail, A.P. Purdy, S. Shafieezad, and R.B. Hallock, *Chem. Mater.* **1**, 4 (1989).
102. M. Guglielmi, A. Martucci, E. Menegazzo, G.C. Righini, S. Pelli, J. Fick, and G. Vitrant, *J. Sol–Gel Sci. Technol.* **8**, 1017 (1997).
103. L. Spanhel, E. Arpac, and H. Schmidt, *J. Non-Cryst. Solids* **147**&**148**, 657 (1992).
104. W.C. Johnson, J.B. Parsons, and M.C. Crew, *J. Phys. Chem.* 36, 2561 (1932).
105. A. Addaniano, *J. Electrochem. Soc.* **108**, 1072 (1961).
106. J.W. Hwang, S.A. Hanson, D. Britton, J.F. Evans, K.F. Jensen, and W.L. Gladfelter, *Chem. Mater.* **7**, 517 (1995).
107. J.E. Andrews and M.A. Littlejohn, *J. Electrochem. Soc.* **122**, 1273 (1975).
108. Y. Xie, Y. Qian, W. Wang, S. Zhang, and Y. Zhang, *Science* **272**, 1926 (1996).
109. O.I. Mićić, S.P. Ahrenkiel, D. Bertram, and A. *J. Nozik, Appl. Phys. Lett.* **75**, 478 (1999).
110. A. Manz, A. Birkner, M. Kolbe, and R.A. Fischer, *Adv. Mater.* **12**, 569 (2000).
111. J.F. Janik and R.L. Wells, *Chem. Mater.* **8**, 2708 (1996).
112. J.L. Coffer, M.A. Johnson, L. Zhang, and R.L. Wells, *Chem. Mater.* **9**, 2671 (1997).
113. R.K. Iler, *The Chemistry of Silica: Solubility, Polymerization, Colloid and Surface Properties*, and Biochemistry, Wiley, New York, 1979.
114. E. Matijević, *Chem. Mater.* **5**, 412 (1993).
115. E. Matijević, *Langmuir* **10**, 8 (1994).
116. S.T. Selvan, C. Bullen, M. Ashokkumar, and P. Mulvaney, *Adv. Mater.* **13**, 985 (2000).
117. F. Caruso, *Adv. Mater.* **13**, 11 (2001).
118. C.J. Brinker and G.W. Scherer, *Sol–Gel Science: The Physics and Chemistry of Sol–Gel Processing*, Academic Press, San Diego, CA, 1990.
119. Alain C. Pierre, *Introduction to Sol–Gel Processing*, Kluwer, Boston, MA, 1998.
120. J.D. Wright and N. A.J.M. Sommerdijk, *Sol–Gel Materials: Chemistry and Applications*, Gordon and Breach Science Publishers, Amsterdam, 2001.

121. J. Livage, F. Babonneau, and C. Sanchez, in *Sol–Gel Optics: Processing and Applications*, ed. L.C. Klein, Kluwer, Boston, MA, p. 39, 1994.
122. B.E. Yoldas, *J. Non-Cryst. Solids* **38–39**, 81 (1980).
123. C.M. Chan, G.Z. Cao, H. Fong, M. Sarikaya, T. Robinson, and L. Nelson, *J. Mater. Res.* **15**, 148 (2000).
124. H. Matsuda, N. Kobayashi, T. Kobayashi, K. Miyazawa, and M. Kuwabara, *J. Non-Cryst. Solids,* **271**, 162 (2000).
125. E. Matijević, *Acc. Chem. Res.* **14**, 22 (1981).
126. E. Matijević, Prog. *Colloid Polym. Sci.* **57**, 95 (1976).
127. W. Stöber, A. Finx, and E. Bohn, *J. Colloid Interf. Sci.* **26**, 62 (1968).
128. E. Matijević and P. Scherner, *J. Colloid Interf. Sci.* **63**, 509 (1978).
129. S. Sun, H. Zeng, D. B. Robinson, S. Raoux, P. M. Rice, S. X. Wang, and X. Guan, *J. Am. Chem. Soc.* **126**, 273 (2004).
130. H. Zeng, P. M. Rice, S. X. Wang, and S. Sun, *J. Am. Chem. Soc.* **126 (37)**, 11458 (2004).
131. E. Matijević and W.P. Hsu, *J. Colloid Interf. Sci.* **118**, 506 (1987).
132. D. Sordelet and M. Akinc, *J. Colloid Interf. Sci.* **122**, 47 (1988).
133. G. Wakefield, E. Holland, P.J. Dobson, and J.L. Hutchison, *Adv. Mater.* **13**, 1557 (2001).
134. E. Matijević, *Ann. Rev. Mater. Sci.* **15**, 483 (1985).
135. E. Matijević, *J. Colloid Interf. Sci.* **58**, 374 (1977).
136. L. Spanhel and M.A. Anderson, *J. Am. Chem. Soc.* **113**, 2826 (1991).
137. S. Sakohara, M. Ishida, and M.A. Anderson, *J. Phys. Chem.* **B102**, 10169 (1998).
138. U. Koch, A. Fojtik, H. Weller, and A. Henglein, *Chem. Phys. Lett.* **122**, 507 (1985).
139. M. Haase, H. Weller, and A. Henglein, *J. Phys. Chem.* **92**, 482 (1988).
140. D.W. Bahnemann, C. Karmann, and M.R. Hoffmann, *J. Phys. Chem.* **91**, 3789 (1987).
141. S.A. Nepijko, D.N. Levlev, W. Schulze, J. Urban, and G. Ertl, *Chem. Phys. Chem* **3**, 140 (2000).
142. E. Wagner and H. Brünner, *Angew. Chem.* **72**, 744 (1960).
143. M. Ohring, *The Material Science of Thin Films, Academic Press*, San Diego, CA, 1992.
144. S.A. Nepijko, H. Hofmeister, H. Sack-Kongehl, and R. Schlögl, *J. Cryst. Growth* **213**, 129 (2000).

145. J. Viereck, W. Hoheisel, and F. Trager, *Surf. Sci.* **340**, L988 (1995).
146. A.E. Romanov, I.A. Polonsky, V.G. Gryaznov, S.A. Nepijko, T. Junghannes, and N.I, Vitryhovski, *J. Cryst. Growth* **129**, 691 (1993).
147. M. Haruta, Catal. *Today* **36**, 153 (1997).
148. R.J.H. Grisel and B.E. Nieuwenhuys, *J. Catal.* **199**, 48 (2001).
149. M. Valden, X. Lai and D.W. Goodman, *Science* **281**, 1647 (1998).
150. P.C. Sercel, W.A. Saunders, H.A. Atwater, and K.J. Vahala, *Appl. Phys. Lett.* **61**, 696 (1992).
151. M. Yamane and Y. Asahara, *Glasses for Photonics, Cambridge University*. Press, Cambridge, 2000.
152. R.H. Doremus, *Glass Science*, 2nd edn., John Wiley and Sons, New York, 1994.
153. S.D. Stookey, *J. Am. Ceram. Soc.* **32**, 246 (1949).
154. R.H. Doremus, in *Nucleation and Crystallization in Glasses and Melts*, The American Ceramic Society, Columbus, OH, p. 117, 1967.
155. R.H. Doremus, *J. Chem. Phys.* **41**, 414 (1965).
156. R.H. Doremus, S.-C. Kao, and R. Garcia, *Appl. Opt.* **31**, 5773 (1992).
157. K. Uchida, S. Kaneko, S. Omi, C. Hata, H. Tanji, Y. Asahara, and A.J. Ikushima, *J. Opt. Soc. Am.* **B11**, 1236 (1994).
158. E. Cordoncillo, J.B. Carda, M.A. Tena, G. Monros, and P. Escribano, *J. Sol–Gel Sci. Technol.* **8**, 1043 (1997).
159. N. Yanagihara, *Chem. Lett.* 305 (1998)
160. N. Yanagihara, K. Uchida, M. Wakabayashi, Y. Uetake, and T. Hara, *Langmuir* **15**, 3038 (1999).
161. Y. Nakao, J. Chem. Soc., *Chem. Commun.* 826 (1993).
162. Y. Nakao, *J. Colloid Interf. Sci.* **171**, 386 (1995).
163. F.W. Billmeyer, *Textbook of Polymer Science*, 3rd edn., John Wiley and Sons, New York, 1984.
164. H.G. Elias, *Macromolecules*, 2nd edn. Plenum, New York, 1984.
165. J.J. Becker, Trans. Am. Inst. Mining Met. *Petrol. Engr.* **209**, 59 (1957).
166. A.E. Berkowitz and P.J. Flanders, *J. Appl. Phys.* **30**, 111S (1959).
167. V.Franco, C.F. Conde, A. Conde, L.F. Kiss, D. Kaptás, T. Kemény, and I. Vincze, *J. Appl. Phys.* **90**, 1558 (2001).
168. H. Change and A. Bard, *J. Am. Chem. Soc.* **113**, 5588 (1991).
169. H. Hövel, Th. Becker, A. Bettac, B. Reihl, M. Tschudy, and E.J. Williams, *J. Appl. Phys.* **81**, 154 (1997).

170. X.Q. Zhong, D. Luniss, and V. Elings, *Surf. Sci.* **290**, 688 (1993).
171. Y.O. Ahn and M. Seidl, *J. Appl. Phys.* **77**, 5558 (1995).
172. A. Stabel, K. Eichhorst-Gerner, J.P. Rabe, and A.R. González-Elipe, *Langmuir* **14**, 7324 (1998).
173. M.P. Zach and R.M. Penner, *Adv. Mater.* **12**, 878 (2000).
174. C.J. Sandroff, J.P. Harbison, R. Ramesh, M.J. Andrejco, M.S. Hegde, D.M. Hwang, C.C. Change, and E.M. Vogel, *Science* **245**, 391 (1989).
175. Ashok K. Ganguli, Aparna Ganguly and Sonalika Vaidya, *Chem. Soc. Rev.* **39**, 474 (2010).
176. M. Boutonnet, J. Kizling, P. Stenius, and G. Maire, *Colloids Surf.* **5**, 209–225 (1982).
177. K. Naoe, C. Petit, and M. P. Pileni, *Langmuir* **24**, 2792 (2008).
178. C. Petit, P. Lixon, and M. P. Pileni, *J. Phys. Chem.* **94**, 1598 (1990).
179. J. Eastoe, M. J. Hollamby, and L. Hudson, *Adv. Colloid Interface Sci.* **128**, 5 (2006).
180. I. Capek, *Adv. Colloid Interface Sci.* 110, 49 (2004).
181. K. Naoe, C. Petit, and M. P. Pileni, *Langmuir* **24**, 2792 (2008) .
182. I. Lisiecki, *J. Phys. Chem.* B **109**, 12231 (2005).
183. A. R. Malheiro, L. C. Varanda, J. Perez, and H. M. Villullas, *Langmuir* **23**, 11015 (2007).
184. J. Ahmed, K. V. Ramanujachary, S. E. Lofland, A. Furiato, G. Gupta, S.M. Shivaprasad, and A.K. Ganguli, *Colloids Surf. A* **331**, 206 (2008).
185. A.K. Ganguli, T. Ahmad, S. Vaidya, and J. Ahmed, *Pure Appl. Chem.* **80**, 2451 (2008).
186. A.K. Ganguli, T. Ahmad, and J. Nanosci. *Nanotechnol.* **7**, 2029 (2007).
187. T. Ahmad, K. V. Ramanujachary, S. E. Lofland, and A. K. Ganguli, *J. Chem. Sci.* **118**, 513 (2006).
188. L. Xiong and T. He, *Chem. Mater.* **18**, 2211 (2006).
189. M. Meyer, C. Wallberg, K. Kurihara, and J.H. Fendler, *J. Chem. Soc. Chem. Commun.* 90 (1984).
190. J.H. Fendler, *Chem. Rev.* **87**, 877 (1987).
191. J.W. Anderson, G.K. Banker, J.E. Drake, and M. Rodgers, *J. Chem. Soc.,* Dalton Trans. 1716 (1973).
192. J.R. Fried, *Polymer Science and Technology*, Prentice Hall, Upper Saddle River, NJ, P. 51, 1995.
193. I Piirma (ed.), *Emulsion Polymerization*, Academic Press, New York, 1982.

194. G.W. Poehlein, R.H. Ottewill, and J.W. Goodwin, (eds.), *Science and Technology of Polymer Colloids*, Vol. II, Martinus Nijhoff, Boston, MA, 1983.
195. R.C. Backus and R.C. Williams, *J. Appl. Phys.* **20**, 224 (1949).
196. E. Bradford and J. Vanderhoff, *J. Appl. Phys.* **26**, 864 (1955).
197. N.A. Fuchs and A.G. Sutugin, in *Aerosol Science*, ed. C.N. Davies, Academic Press, New York, p. 1, 1966.
198. M. Visca and E. Matijević, *J. Colloid Interf. Sci.* **68**, 308 (1978).
199. B.J. Ingebrethsen and E. Matijević, *J. Aerosol Sci.* **11**, 271 (1980).
200. R. Partch, E. Matijević, A.W. Hodgson, and B.E. Aiken, *J. Polymer Sci. Polymer Chem. Ed.* **21**, 961 (1983).
201. K. Nakamura, R.E. Partch, and E. Matijević, *J. Colloid Interf. Sci.* **99**, 118 (1984).
202. N. Herron, Y. Wang, and H. Eckert, *J. Am. Chem. Soc.* **112**, 1322 (1990).
203. M. Chatry, M. In, M. Henry, C. Sanchez, and J. Livage, *J. Sol–Gel Sci. Technol*. **1**, 233 (1994).
204. G.L. Messing, S.C. Zhang, and G.V. Jayanthi, *J. Am. Ceram. Soc.* **76**, 2707 (1993).
205. A. Gurav, T. Kodas, T. Pluym, and Y. Xiong, *Aerosol Sci. Technol.* **19**, 411 (1993).
206. N. Kieda and G.L. Messing, *J. Mater. Res.* **13**, 1660 (1998).
207. J.G. Brennan, T. Siegrist, P.J. Carroll, S.M. Stuczynski, L.E. Brus, and M.L. Steigerwald, *J. Am. Chem. Soc.* **111**, 4141 (1989).
208. K. Osakada and T. Yamamoto, *J. Chem. Soc., Chem. Commun.* 1117 (1987).
209. M.L. Steigerwald and C.R. Sprinkle, *J. Am. Chem. Soc.* **109**, 7200 (1987).
210. Y.C. Kang, H.S. Roh, and S.B. Park, *Adv. Mater.* **12**, 451 (2000).
211. A.M. Testa, S. Foglia, L. Suber, D. Fiorani, LI. Casas, A. Roig, E. Molins, J.M. Grenéche, and J. Tejada, *J. Appl. Phys.* **90**, 1534 (2001).
212. Y. Wang and N. Herron, *J. Phys. Chem.* **91**, 257 (1987).
213. M.G. Bawendi, M.L. Steigerwald, and L.E. Brus, *Annu. Rev. Phys. Chem.* **41**, 477 (1990).
214. H. Masuda, K. Yasui, and K. Nishio, *Adv. Mater.* **12**, 1031 (2000).
215. M.A. Hines and P. Guyot-Sionnest, *J. Phys. Chem.* **100**, 468 (1996).
216. S.A. Majetich and C. Carter, *J. Phys. Chem.* **97**, 8727 (1993).
217. F. Seker, K. Meeker, T.F. Kuech, and A.B. Ellis, *Chem. Rev.* **100**, 2505 (2000).

218. S.T. Selvan, C. Bullen, M. Ashokkumar, and P. Mulvaney, *Adv. Mater.* **13**, 985 (2001).
219. B.O. Dabbousi, J. Rodriguez-Viejo, F.V. Mikulec, J.R. Heine, H. Mattoussi, R. Ober, K.F. Jensen, and M.G. Bawendi, *J. Phys. Chem.* **B101**, 9463 (1997).
220. X. Peng, M.C. Schlamp, A.V. Kadavanich, and A.P. Alivisatos, *J. Am. Chem. Soc.* **119**, 7019 (1997).